8-14-2014 12:00 AM

# Mutations at the 46th residue change properties of Cx50 gap junction channels

Xiaoling Tong, *The University of Western Ontraio*

Supervisor: Donglin Bai, *The University of Western Ontario*
A thesis submitted in partial fulfillment of the requirements for the Master of Science degree in Physiology

Mutations at the 46$^{th}$ residue change properties of Cx50

gap junction channels

(Thesis format: Integrated paper)

by

Xiaoling <u>Tong</u>

Graduate Program in Physiology and Pharmacology

A thesis submitted in partial fulfillment of the requirements
for the degree of Master of Science

The School of Graduate and Postdoctoral Studies
The University of Western Ontario,
London, Ontario, Canada

# Abstract

The interface of the first transmembrane domain and the first extracellular loop (TM1/E1 border) in several gap junction (GJ) channels is known to line a portion of the pore and plays an important role in determining GJ channel properties. By introduction of a charged residue into this domain of Cx50, the resultant mutant channels showed drastically altered unitary conductance ($\gamma_j$) and transjunctional voltage-dependent gating ($V_j$-gating). Specifically G46D and G46E increased the Cx50 $\gamma_j$ from 201 to 256 and 293 pS, respectively and G46K channel showed a decreased $\gamma_j$ of only 20 pS. Moreover, in single channel recordings of homotypic G46K and heterotypic Cx50/G46K channels, only loop gating transitions were observed, indicating an apparent loss of fast $V_j$-dependent gating transitions. The homology structural models indicate that the pore surface electrostatic potential at the TM1/E1 border is a dictating factor in determining efficiency of ion permeation and $V_j$-gating of Cx50 GJ channels.

**Keywords:** gap junction channel, single channel conductance, connexin50, voltage-dependent gating, patch clamp

# Dedication

I'd like to dedicate this to my husband, who has given up a lot of things to accompany me here and is giving me support and encouragement all the time.

## Statement of Co-authorship

The whole work was accomplished by Xiaoling Tong except the homology models for the gap junction channels of wide-type Cx50, mutants G46D, G46E and G46K, which were constructed by Dr. Hiroshi Aoyama and Dr. Tomitake Tsukihara from Osaka University in Japan.

# Acknowledgements

I'd like to thank my supervisor Dr. Donglin Bai at first, who gave me the opportunity to work in his lab and kept me going when times were tough. He showed great patience in guiding me and offering invaluable advices during the process. I also greatly appreciate the insightful suggestions and evaluations from my advisory committee meeting members Dr. Stan Leung and Dr. Stephen Sims. Moreover, the lab members in both Bai lab and Laird lab are always very supportive and we enjoyed a great time together. Thank you all for the help in the past two years!

# Table of Contents

## Chapter 1: Introduction

# Chapter 2: Article

# Chapter 3: Discussion

# List of Table

# List of Figures

# List of Abbreviations

| | |
|---|---|
| *A* | slope of the Boltzmann fitting curve |
| **CL** | cytoplasmic loop |
| **CsGlu** | cesium glutamate |
| **CT** | carboxyl-terminus |
| **Cx** | connexin |
| **E1** | first extracellular loop |
| **E2** | second extracellular loop |
| **ECF** | extracellular fluid |
| **EGFP** | enhanced green fluorescent protein |
| **EGTA** | ethylene glycol tetraacetic acid |
| **GJ** | gap junction |
| $G_j$ | junctional conductance |
| $G_{j,ini}$ | initial transjunctional conductance |
| $G_{j,ss}$ | normalized steady-state conductance |
| $G_{max}$ | Boltzmann fitting parameters describing maximum normalized conductance |
| $G_{min}$ | Boltzmann fitting parameters describing normalized voltage-insensitive residual conductance |
| **ICF** | intracellular fluid |
| **Ij** | macroscopic junctional current |
| **ij** | junctional current of single channel |
| **MTS** | methanthiosulfonate |
| **ms** | millisecond |
| **N2A** | mouse neuroblastoma cells |
| **nS** | nanoSiemens |

| | |
|---|---|
| **NT** | amino-terminus |
| **Pc** | probability of the channel at fully closed state |
| **Po** | probability of the channel at open state |
| **Ps** | probability of the channel at subconductance state |
| **pS** | picoSiemens |
| **SEM** | standard error of the mean |
| **TEACl** | tetraethylammonium chloride |
| **TM** | transmembrane domain |
| $\mathbf{V_0}$ | Boltzmann fitting parameters describing voltage at which the conductance is reduced by half |
| $\mathbf{V_j}$ | transjunctional voltage |
| $\mathbf{+V_j}$ | positive transjunctional voltage |
| $\mathbf{-V_j}$ | negative transjunctional voltage |
| $\mathbf{V_m}$ | transmembrane voltage |
| $\mathbf{\gamma_j}$ | unitary channel conductance |
| $\mathbf{\tau}$ | time constant |

# Chapter 1: Introduction

## 1.1    Gap junction channels

Connexin (Cx) proteins are the subunits that form gap junction (GJ) channels. To date, 21 connexin isoforms have been identified in humans and 20 in mice. All of them share the same topology with four transmembrane domains (TM1~TM4), two extracellular loops (E1 & E2), one cytoplasmic loop (CL), and both amino-terminus (NT) and carboxyl-terminus (CT) on the cytoplasmic side (Milks, Kumar et al. 1988). Six identical/different connexins are oligomerized into a homomeric/heteromeric hemichannel, respectively. After trafficking to the plasma membrane, the hemichannel can dock to an opposed identical/different hemichannel from a neighboring cell to form a homotypic/heterotypic GJ channel, respectively (Fig. 1.1). The flexibility to organize different connexins into one GJ channel substantially increases functional diversity to meet specific physiological requirements in different cells.

The basic function of GJ channels is to allow direct intercellular communication between two coupled cells. Ions, metabolites (e.g. ATP, glucose), second messengers (e.g. IP3, cGMP) and small interference RNA up to a molecular mass around 1 kDa can pass through the channel with a relatively low selectivity (Loewenstein 1981; Harris 2001). In different tissues and organs, GJ channels serve different purposes. In electrically excitable cells, like cardiomyocytes, smooth muscles and neurons, GJ channels are essential for the instantaneous propagation of electrical impulses and the coordinated responses of effective cell groups in order to generate electrical or mechanical output. In addition to these functions, the substance exchange through GJ channels plays an important role in maintaining cell homeostasis, controlling cell

development, differentiation and apoptosis in a variety of tissues (Goodenough and Paul 2009; Herve and Derangeon 2013).

The factors that are effective in modulating GJ channel functions can be divided into two categories, chemical and electrical. The chemical category mainly includes cytoplasmic pH level, intracellular calcium concentration ($[Ca^{2+}]_i$) and phosphorylation status of connexin proteins, which influence the channel functions directly and/or indirectly. For instance, low intracellular pH is suggested to trigger the pH gating of GJ channels directly by protonation of connexins (Trexler, Bukauskas et al. 1999), or indirectly by protonation of aminosulfonates (Bevans and Harris 1999) and increased $[Ca^{2+}]_i$ (Lazrak and Peracchia 1993), which could subsequently induce the interactions between calmodulins and intracellular domains of connexins (Peracchia, Bernardini et al. 1983; Zhou, Yang et al. 2007; Dodd, Peracchia et al. 2008; Sun, Hills et al. 2014). Connexin phosphorylation is a factor that not only regulates the trafficking, assembling, internalization and degradation of GJ channels, but also has direct effects on the existing GJ channels in the plasma membrane. For example, enhancing the phosphorylation status of Cx43 led to substantially reduced unitary conductance ($\gamma_j$) of the Cx43 GJ channel (Moreno, Saez et al. 1994; Kwak, Saez et al. 1995).

In addition to these chemical factors, the electrical potential differences across the cytosols of two coupled cells (the transjunctional voltage, known as $V_j$) and across the plasma membrane (the transmembrane voltage, known as $V_m$) are also able to modulate the functions of GJ channels. It is noted that only a few GJ channels (e.g. Cx26 and Cx43) are sensitive to $V_m$ (Barrio, Revilla et al. 2000; Revilla, Bennett et al. 2000), while all presently identified GJ channels are gated by $V_j$. Although $V_j$-gating kinetics and $V_j$-sensitivities are widely disparate among different GJ channels, a

2

common feature is that with the application of a continuous $V_j$ pulse, the conductance of most GJ channels is maximum at the initial point of $V_j$ and then gradually decreased to a steady state with residual conductance (termed 'subconductance state'). In the macroscopic records of homotypic GJ channels, positive and negative $V_j$s would generate symmetric current reduction traces due to the identical channel characteristics of two coupled hemichannels. The dependence of junctional conductance ($G_j$) on positive or negative $V_j$s can be described by a two state Boltzmann function independently, in which the ratio of steady state conductance ($G_{ss}$) to initial conductance ($G_{ini}$) is plotted to the corresponding $V_j$, yielding three parameters to describe the $V_j$-gating properties of the GJ channel.
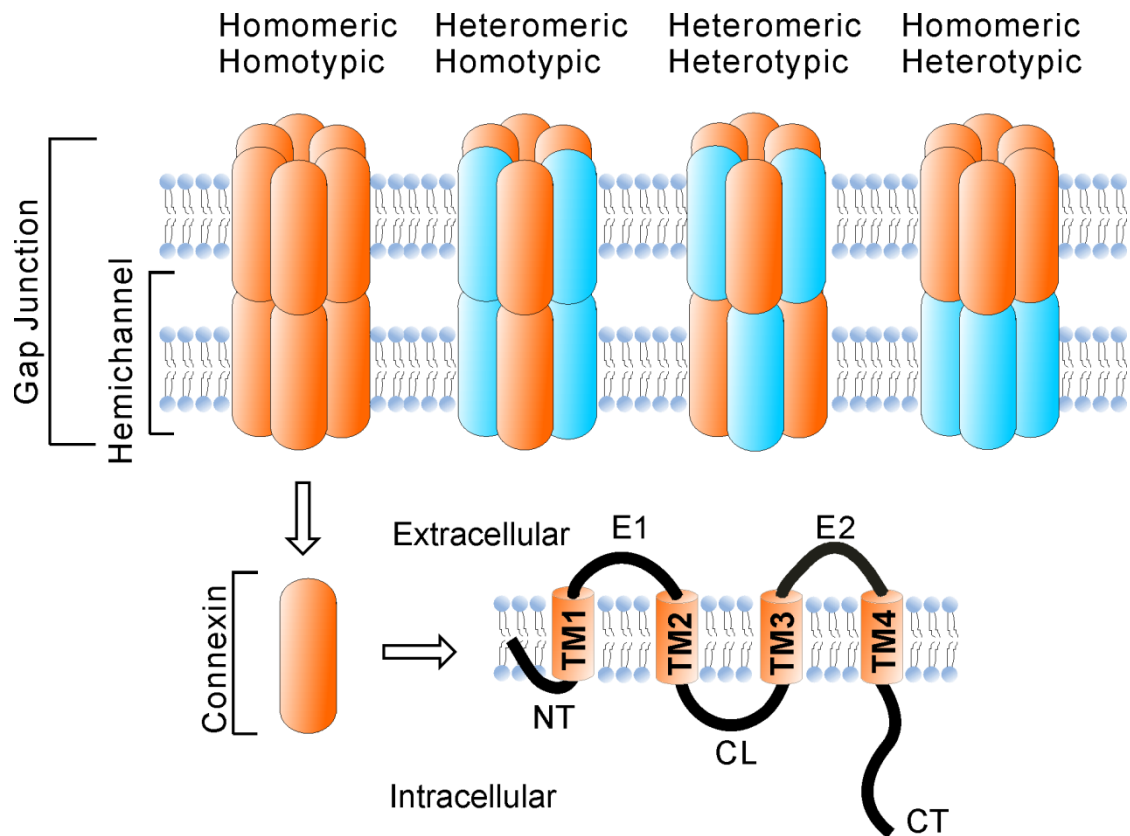
**Figure 1.1** **Various compositions of GJ channels and the topology of a single connexin subunit.** Six identical connexin subunits are oligomerized into a homomeric hemichannel, while differing connexin subunits form a heteromeric hemichannel. Two identical or different hemichannels are docked head-to-head to construct a homotypic or heterotypic GJ channel, respectively. Of these four configurations, there is no solid evidence for the existence of heteromeric homotypic GJ channels in vivo. All connexin isoforms are transmembrane proteins with the same topology.

## 1.2    $V_j$-dependent gating mechanisms

With the application of sufficient $V_j$ across two coupled cells, single channel records of various GJ channels showed the existence of a main open state, one or multiple subconductance states and a fully closed state, as well as two types of gating transitions between these states: fast gating and loop gating (also named slow gating), which were primarily distinguished by their transition times (Bukauskas, Elfgang et al. 1995; Trexler, Bennett et al. 1996; Valiunas, Manthey et al. 1999). Fast gating is characterized by the fast gating transition (the transition time is generally < 2 ms) between the main open state and a subconductance state whose conductance is 5 ~ 40% of the maximum conductance (Trexler, Bennett et al. 1996; Bukauskas and Verselis 2004). The slow or loop gating is characterized by the slow entry (usually takes several to tens of milliseconds) of the channel into the fully closed state.

These two gating components exist simultaneously in a hemichannel with distinct sensitivities to $V_j$. In a typical GJ channel, two hemichannels are docked head-to-head, aligning two fast gates and two loop gates in series. Their responses to $V_j$ follow the contingent gating model in which the state of one gate largely depends on the states of other gates (Moreno, Laing et al. 1995; Bukauskas, Angele et al. 2002; Paulauskas, Pranevicius et al. 2009). When applying sufficient $V_j$, the closure of one fast gate cuts off the $V_j$ gradient across the entire channel drastically, resulting in the lasting opening of the opposed fast gate. The $V_j$-sensitivity of loop gating is much lower than that of fast gating; thus in most GJ channels, including Cx50, the loop gating activity is very scarce.

A prominent property of the fast gate is its $V_j$-gating polarity, which describes the closure of the gate on the cytoplasmic side with either relatively positive or negative potential, depending on the connexin type that forms the GJ channels. For

5

instance, of two mirrored fast gates in a Cx50 GJ channel, only the fast gate on the cytoplasmic side with relative positive $V_j$ is closed; therefore, its gating polarity is positive (Fig. 1.2). In contrast to Cx50, fast gating in Cx32 and Cx43 GJ channels exhibited negative gating polarity (Chen-Izu, Moreno et al. 2001; Abrams, Freidin et al. 2006). Loop gating also has polarity, but in all currently studied connexin members, loop gating only occurrs at the inside negative potential, which means that its gating polarity is always negative (Oh, Abrams et al. 2000; Verselis, Trexler et al. 2000; Bukauskas, Angele et al. 2002).

The facts that fast and loop gatings are different in their gating transition times and have different polarities in some GJ channels imply the existence of distinct voltage sensors/gates for these two gating mechanisms. So far, evidence is not solid to interpret the relationship between $V_j$ sensors and gates, as well as their locations in GJ channels, yet a widely accepted opinion is that sensors of these two gatings all reside in the channel lumen in order to sense $V_j$ efficiently. A crystal structure of an open state of Cx26 GJ channels was resolved at 3.5 Å resolution in 2009, showing that the inner wall of the channel was composed of NT, the first half of E1 and the second half of TM1 domains of each connexin (Maeda, Nakagawa et al. 2009; Nakagawa, Maeda et al. 2010). These pore-lining domains are critical in determining $\gamma_j$ and $V_j$-gating properties of GJ channels because they not only shape the pore, but are also capable of sensing the changes of $V_j$ field directly.
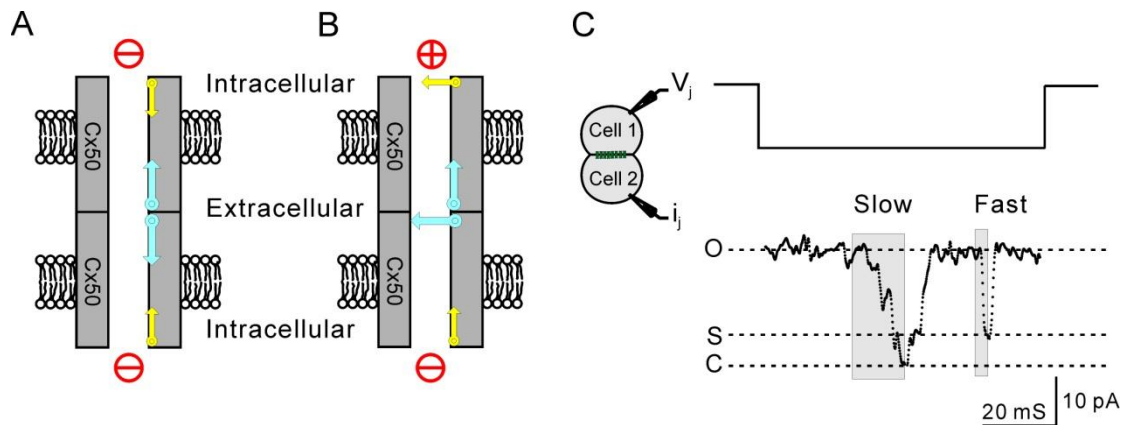
**Figure 1.2   Fast and loop gating polarities in Cx50 GJ channels and a representative single channel recording.** A) A cartoon representation of a side view of a functional GJ channel spanning two neighboring cells. Each hemichannel possesses one fast gate (yellow arrow) on the cytoplasmic side likely formed by NT, and one loop gate (blue arrow) on the extracellular side possibly involving the TM1/E1 border. While two cells have an equal intracellular potential ($V_j = 0$), all fast and slow gates continue to remain open. B) When the cytoplasmic potential on the top side becomes relatively positive compared to the bottom side, fast gate on the positive side (positive polarity) closes the channel to a subconductance state. Loop gate on the negative side (negative polarity) is able to close the channel completely albeit with a much lower $V_j$ sensitivity. C) In a typical voltage-clamp record of Cx50 GJ channel, fast gate closes the channel from a main open state to a subconductance state with a rapid single-step transition, while loop gate normally fully closes the channel in a multi-step process. O: open state; S: subconductance state; C: fully closed state.

### 1.2.1 Structural basis for fast gating

In most GJ channels, fast gating is the dominant component in response to $V_j$ because of its higher $V_j$ sensitivity than that of loop gating. A number of structure-function studies using site-directed mutagenesis or domain swapping method identified the NT domain as a possible voltage sensor and gate in fast gating. In 1994, Bargiello and colleagues reported that the fast gating polarities of Cx26 and Cx32 channels were reversed simply by changing the charge status of the $2^{nd}$ amino acid residue in the NT of these two connexins (Verselis, Ginter et al. 1994). A further study on Cx32 using the same methods extended the effective residues to the $5^{th}$, $8^{th}$ and $10^{th}$ amino acids, giving a conclusion that the first 10 residues of NT reside inside the pore, which allow the exclusive sensitivity to $V_j$ field and not $V_m$ (Oh, Rivkin et al. 2004). Similar results were observed in both Cx46 and Cx50, as mutating the negatively charged residue Asp3 to neutral Asn (D3N) reversed their gating polarity from positive to negative (Peracchia and Peracchia 2005; Srinivas, Kronengold et al. 2005).

The high resolution (3.5 Å) crystal structure of Cx26 GJ published later on provides a structural basis for these earlier findings (Maeda, Nakagawa et al. 2009). In this structure, the NTs of six Cx26 monomers in a hemichannel are folding back into the channel, forming a constricted pore entrance with their NT helices. At open state, their positions are stabilized by intra-subunit hydrophobic bonds between Trp3 and Met 34 as well as inter-subunit hydrogen bonds between Asp2 and Thr5. However, they are still relatively flexible compared to other components in the channel and possibly driven by $V_j$ to move towards the cytoplasm which would consequently close the channel to a subconductance state. A study in a heteromeric channel by Oh S. and colleagues suggested that the movement of a single NT subunit rather than the

concerted action of 6 subunits is sufficient to clog the channel (Oh, Abrams et al. 2000). Due to the absence of high-resolution crystal structure for the closed state of any GJ channel, how exactly the conformation changes are triggered by the fast gating is still an open question. Electrophysiology data provide conjectures but are far from being conclusive.

### 1.2.2 Structural basis for loop gating

The slow/loop gating observed in both GJ channels and undocked hemichannels is possibly responsible for the opening of newly docked GJ channels and the securing closure of undocked hemichannels in the plasma membrane to prevent leakage and dilution of cytoplasmic contents (Trexler, Bennett et al. 1996; Bukauskas, Angele et al. 2002; Bukauskas and Verselis 2004; Rackauskas, Kreuzberg et al. 2007). The gating transition features a stepwise conductance reduction, usually taking tens of milliseconds to achieve, and can fully close the channel from the main open state or a subconductance state (Bukauskas, Bukauskiene et al. 2001; Oh, Rivkin et al. 2004). Unlike fast gating, loop gating of all characterized GJ channels displays negative gating polarity and less sensitivity to $V_j$. Currently, most studies of loop gating are conducted on undocked hemichannels rather than GJ channels most likely for the reason that a hemichannel normally only possesses two gating components (one fast gate and one loop gate) instead of four symmetric gating components in a GJ channel (two fast gates and two loop gates). However, whether the properties of loop gating in a hemichannel are the same as those in a GJ channel is still an unsolved question.

The boundary sequence between the first transmembrane domain and the first extracelluar loop (TM1/E1 border) is believed to be a possible voltage sensor and gate, or at least an energy barrier for the loop gating (Kronengold, Trexler et al. 2003;

Verselis, Trelles et al. 2009). Earlier studies also identified that residue substitutions at the TM1/E1 border were capable of altering GJ channel properties, including $\gamma_j$, charge permeability and gating polarity (Verselis, Ginter et al. 1994; Hu and Dahl 1999; Trexler, Bukauskas et al. 2000; Hu, Ma et al. 2006). In the crystal structure of Cx26 GJ channels, a parahelix structure (ranging from residue 42 to 51) at the TM1/E1 border functionally exposes a few acidic residues toward the pore surface and constructs a negatively charged pathway (Maeda, Nakagawa et al. 2009). Sequence alignment reveals that these negatively charged residues at the TM1/E1 border of Cx26 are well conserved in most other connexins (Maeda and Tsukihara 2011), indicating the existence of a similar negatively charged pathway in most GJ channels which would serve similar functions, including a voltage sensor for the loop gating, or to influence gating polarity and ion preference with the prominent local negative surface electrostatic potential.

At the resting membrane potential, loop gating is responsible for closing unopposed hemichannels in the plasma membrane to preserve intracellular homeostasis. The closing process driven by $V_m$ in undocked Cx50 and Cx32*Cx43E1 hemichannels showed multiple (4~6) steps, which was interpreted as the involvement of up to 6 connexin subunits one-by-one at their TM1/E1 borders (Tang, Dowd et al. 2009; Verselis, Trelles et al. 2009). It is suggested that the parahelix structure at the TM1/E1 border would experience rotation and/or tilt toward the pore center during the loop gating process, which would occlude the channel completely if all 6 connexin subunits are enrolled. Moreover, the closely-located residues in the parahelices could form low-affinity metal chelating sites for divalent cations (e.g. $Ca^{2+}$, $Cd^{2+}$, $Mg^{2+}$) to further stabilize the fully closed state. On the contrary, removing the extracellular $Ca^{2+}$ resulted in an increased opening of hemichannels in the plasma membrane,

showing increased hemichannel current in electrophysiological recording and up-regulated dye-uptake (Trexler, Bennett et al. 1996; Srinivas, Calderon et al. 2006; Verselis, Trelles et al. 2009).

### 1.2.3 Other conformation changes related to $V_j$-dependent gating

Most studies indicate that in a GJ channel, NT serves a dual purpose as both the $V_j$ sensor and gate for fast gating, and the TM1/E1 border domain is a possible sensor and gate for loop gating. However, there are also other conformation changes closely associated with the $V_j$-dependent gating. A highly conserved proline (P87) residue was identified in the middle of an α-helix structure in TM2 domain across members of connexin family, which is well known for its function to form a kink in a transmembrane helix (Sankararamakrishnan and Vishveshwara 1992). Several mutations at P87 in Cx26 and T86 in Cx32, purposely modifying the flexibility and bending angle of TM2 helices to various degrees, showed altered $V_j$ gating properties and gating polarities, suggesting that the conformation changes of TM2 are also related to the $V_j$-dependent gating (Suchyna, Xu et al. 1993; Ri, Ballesteros et al. 1999). Another theory proposed in Cx40 and Cx43 GJ channels is similar to the "ball and chain" model of voltage-dependent ion channels, e.g. voltage-dependent sodium channel and shaker potassium channel (Armstrong and Bezanilla 1977; Hoshi, Zagotta et al. 1990), based on the observation that removing the CT of Cx40 and Cx43 eliminated the fast gating and subconductance states in their GJ channels, while co-expressing an independent CT peptide could restore these properties (Revilla, Castro et al. 1999; Anumonwo, Taffet et al. 2001; Moreno, Chanson et al. 2002). Further research suggested that the CT of Cx43 possibly binds its CL and forms a particle-receptor structure to clog the channel (Shibayama, Gutierrez et al. 2006). This

is inconsistent with recently postulated conformational changes of fast gating in other connexins, like Cx26, Cx32 and Cx50, all of which suggest the involvement of NT as both the sensor and fast gate simultaneously. However, it is also possible that this "ball and chain" theory is unique to Cx40 and Cx43 GJ channels.

## 1.3    Heterotypic GJ channels

A heterotypic GJ channel is formed by the head-to-head docking of two hemichannels with different connexin compositions. Compared to homotypic GJ channels, many questions pertaining heterotypic GJ channels remain unsolved. The co-localization of various connexins in the same tissue or organ makes it possible for different types of connexins to oligomerize and form heteromeric hemichannels and heterotypic GJ channels. The unique properties of heterotypic channels compared to homotypic channels are crucial to meet special physiological requirements. One of their prominent features is to mediate asymmetric chemical and/or electrical signaling between two cells, which is largely determined by the properties of each hemichannel. For example, in a homomeric heterotypic Cx32/Cx26 GJ channel, two fast gates were closed simultaneously when a relatively positive $V_j$ was applied to the Cx26 side, but neither of them reacted to a relatively positive potential on the Cx32 side, owing to the opposite fast gating polarities between Cx32 (negative) and Cx26 (positive) hemichannels (Verselis, Ginter et al. 1994). In addition to this, the Cx26/Cx32 channel showed a strong rectified $\gamma_j$. The application of positive $V_j$ on the Cx26 side clearly produced a much higher current amplitude than negative $V_j$, indicating that the current flows more readily from the Cx26 hemichannel to the Cx32 hemichannel than in the opposite direction (Oh, Rubin et al. 1999; Suchyna, Nitsche et al. 1999). A possible explanation for this phenomenon is the asymmetric structures of two coupled

hemichannels, especially their distinct distributions of charged residues in the pore surface, which may substantially result in an unequal ability to conduct ions. In our study, in order to investigate the properties of G46K mutant, we constructed heterotypic Cx50/G46K GJ channels. In this channel, because the $V_j$-gating properties of Cx50 GJ channels and hemichannels have been well documented, the appearance of new features can be ascribed to the opposed G46K hemichannel. The heterotypic Cx50/G46K channel exhibited asymmetric $V_j$-dependent gating and significant instantaneous rectification. By using the homology structure models of Cx50 GJ channel and mutants G46D/E/K, we were able to compare their channel structures, especially the surface electrostatic fields at the TM1/E1 border to identify the possible structural basis for their specific features.

## 1.4 Connexin 50

### 1.4.1 Localization and physiological functions

Cx50 is one of the best studied connexin members. It is exclusively expressed in vertebrate lens together with two other connexins, Cx43 and Cx46, in a partially overlapping manner (Beyer, Kistler et al. 1989; Paul, Ebihara et al. 1991; White, Bruzzone et al. 1992). The lens is an avascular organ constituted by multiple cell layers; therefore, high-density GJ channels are vital to provide low-resistance pathways for the entry and exit of water, ions, nutrients, metabolites and other physiological substances between cells. The expression of Cx43 is restricted in epithelial cells (the outmost layers), while Cx46 is in the core of the lens, which is constructed by differentiating and mature fiber cells. Cx50 is expressed in the whole lens, but with different forms. During the maturation of human and mouse fiber cells, CT of Cx50 was naturally truncated at position 290 or 294, but the truncated form was

still able to compose functional GJ channels (DeRosa, Mui et al. 2006). The physiological differences between these two forms of Cx50 are unclear.

Notably, Cx50 knock-out mice had not only small eyes and lenses, termed microphthalmia, but they also developed cataract at an early age (White, Goodenough et al. 1998; Rong, Wang et al. 2002; Sellitto, Li et al. 2004). Therefore, Cx50 is crucial in promoting cell proliferation and differentiation, as well as maintaining lens homeostasis and transparency. Its functions cannot be fully compensated by an over expression of Cx46, as Cx46 knock-in mice (replace Cx50 gene locus with Cx46) still had undersized lenses despite being transparent (Mathias, White et al. 2010). Up to date, dozens of missense and frame shift mutations of the Cx50 gene have been identified as one of the underlying causes for inherited cataracts in both human families and mouse models (Chang, Wang et al. 2002; Sun, Xiao et al. 2011; Beyer, Ebihara et al. 2013). Most of these mutants exhibited a loss of GJ channel functions mainly due to failed trafficking to the plasma membrane, unsuccessful docking or channel opening issues (Arora, Minogue et al. 2008; Berthoud, Minogue et al. 2013; Sun, Hills et al. 2014). The residue localizations of these human mutations are depicted in a schematic diagram of Cx50 in Fig. 1.3, which was summarized from Beyer's review and Zhang's paper (Beyer, Ebihara et al. 2013; Ge, Zhang et al. 2014).

### 1.4.2 Structure-function studies of Cx50

The Cx50 GJ channel is highly sensitive to $V_j$ and intracellular pH (Lin, Eckert et al. 1998; Srinivas, Costa et al. 1999). Its $\gamma_j$ is around 200 pS, one of the largest among connexin isoforms. Extensive studies have been carried out on its NT domain and identified its role as one of the principal domains to determine the $V_j$-gating properties and $\gamma_j$ (Tong, Liu et al. 2004; Peracchia and Peracchia 2005; Xin, Gong et

al. 2010). Replacing the $3^{rd}$ residue in NT, a negatively charged Asp (D) with a neutral Asn (N) reversed its fast gating polarity from positive to negative (Peracchia and Peracchia 2005). Moreover, mutant Cx50-D3E, which preserved the negative charge at this position but with a slightly prolonged side chain, dramatically reduced its $\gamma_j$ and changed its open-closed stability, suggesting a pivotal role of this residue position in determining channel properties (Xin, Nakagawa et al. 2012).

Cx50 has a huge CT domain with more than 200 residues, yet CT-cleaved Cx50 showed similar $V_j$-dependent gating as wild type, but with lower $\gamma_j$ (DeRosa, Mui et al. 2006). Controversial results were obtained in terms of the impact of CT truncation on pH gating. Some reports found that even without CT, the Cx50 GJ channel preserved high sensitivity to cytoplasmic pH (Lin, Eckert et al. 1998; Xu, Berthoud et al. 2002), whereas another paper found that its pH gating was damaged after the removal of CT (DeRosa, Mui et al. 2006).

In addition to NT and CT, TM1/E1 border is another key functional domain in Cx50 GJ channels. A careful inspection of the distribution of cataract-related mutants in Cx50 found that the TM1/E1 border demonstrated the highest incidence of point mutations and most of them are fatal to channel operation (Fig. 1.3). This implies that the structure and function of this domain are strictly defined and have little tolerance to residue alteration. In the crystal structure of Cx26 GJ, the TM1/E1 border domain has following features: 1) It is pore-lining and constructs the second narrowest part in an open GJ channel, slightly wider than the NT funnel; 2) The pore surface of this part is enriched by circles of negatively charged residues; 3) A parahelix structure (from residue 42 to 51) is likely involved in loop gating. Even though the Cx50 crystal structure is currently not available, hemichannel studies of Cx50 identified that every 3-5 residues at the TM1/E1 border are pore-lining (including F43, G46 and D51) in a

pattern similar to Cx26, suggesting the existence of a parahelix structure as Cx26 (Verselis, Trelles et al. 2009). Meanwhile, Cx50 contains more negatively charged residues in this domain than Cx26 and most of them are located at the equivalent positions as those of Cx26. In this study, in order to examine the role of TM1/E1 border in determining Cx50 GJ properties, we replaced the neutral G46 with charged residues to modify the local electrostatic field to more negative or less negative. Compared to other residues at the TM1/E1 border, G46 is one of the residues predicted to face the pore directly (Verselis, Trelles et al. 2009), therefore its mutations would modify the local electrostatic potential easily. Moreover, it is not a critical structural residue because mutants on this site are more likely to form functional GJ channels, which would make our further structure-function studies possible (Mese, Sellitto et al. 2011; Tong, Minogue et al. 2011). Homology structural models of the Cx50 GJ channel and its mutants G46D/E/K were generated based on the crystal structure of Cx26 GJ channel for possible interpretations of our electrophysiological data with structural mechanisms.
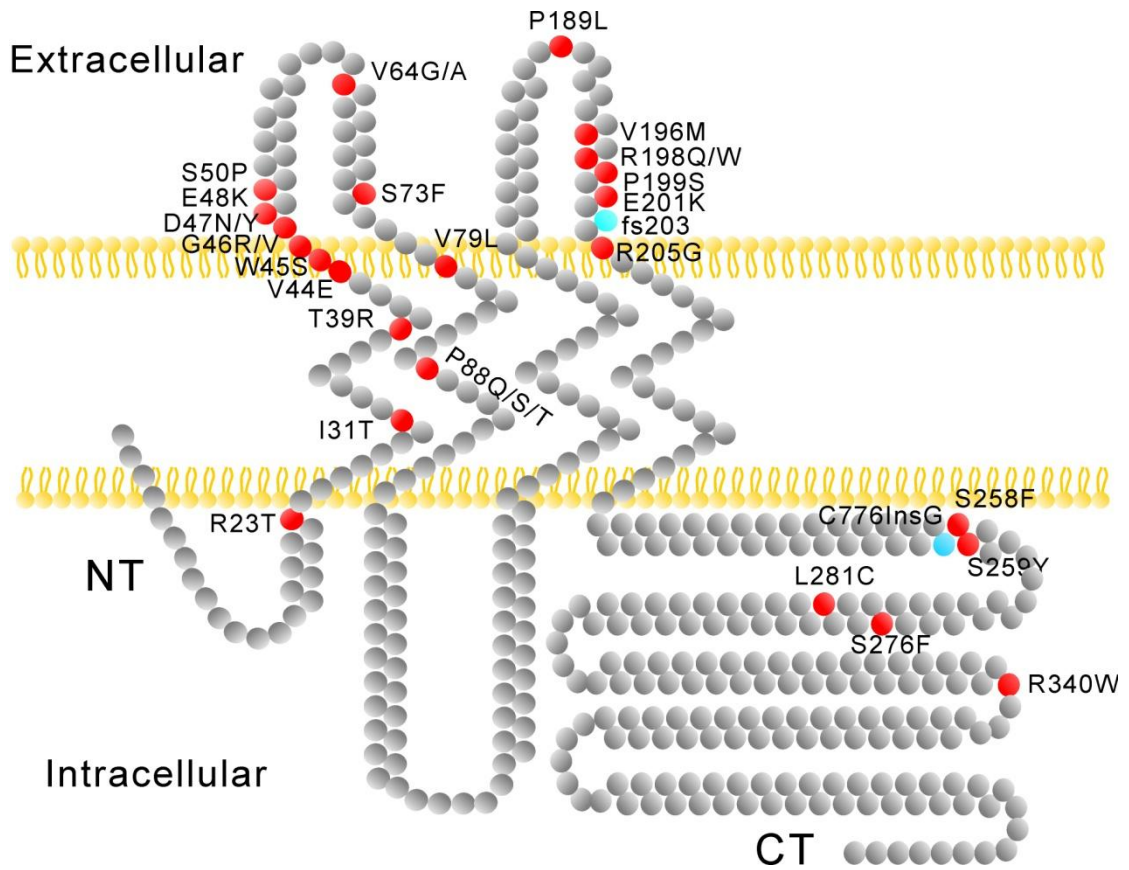
**Figure 1.3** **A schematic diagram summarizes currently identified cataract-linked Cx50 mutations.** Red: missense mutants; Blue: a single base insertion leading to frame shift.

## 1.5    Hypothesis

By mutating a pore lining residue G46 at the TM1/E1 border into a negatively charged residue aspartic acid (D) or glutamate acid (E), or a positively charged residue lysine (K), the Cx50 GJ channel would show altered $\gamma_j$, $V_j$-gating properties and cation/anion preference.

## 1.6    Objectives

1) To explore the role of surface charges at the TM1/E1 border in determining the $\gamma_j$ of Cx50 GJ channel by replacing uncharged G46 with charged residues D, E or K.

2) To identify the role of surface charges at the TM1/E1 border in determining the $V_j$-gating behavior of Cx50 GJ channel.

3) To investigate whether the cation-favoring property of Cx50 GJ channel is related to the high-density negative surface charges at the TM1/E1 border.

## 1.7 References

Abrams, C. K., M. M. Freidin, et al. (2006). "Properties of human connexin 31, which is implicated in hereditary dermatological disease and deafness." <u>Proc Natl Acad Sci U S A</u> **103**(13): 5213-5218.

Anumonwo, J. M., S. M. Taffet, et al. (2001). "The carboxyl terminal domain regulates the unitary conductance and voltage dependence of connexin40 gap junction channels." <u>Circ Res</u> **88**(7): 666-673.

Armstrong, C. M. and F. Bezanilla (1977). "Inactivation of the sodium channel. II. Gating current experiments." <u>J Gen Physiol</u> **70**(5): 567-590.

Arora, A., P. J. Minogue, et al. (2008). "A novel connexin50 mutation associated with congenital nuclear pulverulent cataracts." <u>J Med Genet</u> **45**(3): 155-160.

Barrio, L. C., A. Revilla, et al. (2000). "Membrane potential dependence of gap junctions in vertebrates." <u>Gap Junctions</u> **49**: 175-188.

Berthoud, V. M., P. J. Minogue, et al. (2013). "Connexin50D47A decreases levels of fiber cell connexins and impairs lens fiber cell differentiation." <u>Invest Ophthalmol Vis Sci</u> **54**(12): 7614-7622.

Bevans, C. G. and A. L. Harris (1999). "Regulation of connexin channels by pH. Direct action of the protonated form of taurine and other aminosulfonates." <u>J Biol Chem</u> **274**(6): 3711-3719.

Beyer, E. C., L. Ebihara, et al. (2013). "Connexin mutants and cataracts." <u>Front Pharmacol</u> **4**: 43.

Beyer, E. C., J. Kistler, et al. (1989). "Antisera directed against connexin43 peptides react with a 43-kD protein localized to gap junctions in myocardium and other tissues." <u>J Cell Biol</u> **108**(2): 595-605.

Bukauskas, F. F., A. B. Angele, et al. (2002). "Coupling asymmetry of heterotypic connexin 45/ connexin 43-EGFP gap junctions: properties of fast and slow gating mechanisms." <u>Proc Natl Acad Sci U S A</u> **99**(10): 7113-7118.

Bukauskas, F. F., A. Bukauskiene, et al. (2001). "Gating properties of gap junction channels assembled from connexin43 and connexin43 fused with green fluorescent protein." <u>Biophys J</u> **81**(1): 137-152.

Bukauskas, F. F., C. Elfgang, et al. (1995). "Biophysical properties of gap junction channels formed by mouse connexin40 in induced pairs of transfected human HeLa cells." <u>Biophys J</u> **68**(6): 2289-2298.

Bukauskas, F. F. and V. K. Verselis (2004). "Gap junction channel gating." <u>Biochim Biophys Acta</u> **1662**(1-2): 42-60.

Chang, B., X. Wang, et al. (2002). "A Gja8 (Cx50) point mutation causes an alteration of alpha 3 connexin (Cx46) in semi-dominant cataracts of Lop10 mice." <u>Hum Mol Genet</u> **11**(5): 507-513.

Chen-Izu, Y., A. P. Moreno, et al. (2001). "Opposing gates model for voltage gating of gap junction channels." <u>Am J Physiol Cell Physiol</u> **281**(5): C1604-1613.

DeRosa, A. M., R. Mui, et al. (2006). "Functional characterization of a naturally occurring Cx50 truncation." <u>Invest Ophthalmol Vis Sci</u> **47**(10): 4474-4481.

Dodd, R., C. Peracchia, et al. (2008). "Calmodulin association with connexin32-derived peptides suggests trans-domain interaction in chemical gating of gap junction channels." J Biol Chem **283**(40): 26911-26920.

Ge, X. L., Y. Zhang, et al. (2014). "Identification of a novel GJA8 (Cx50) point mutation causes human dominant congenital cataracts." Sci Rep **4**: 4121.

Goodenough, D. A. and D. L. Paul (2009). "Gap junctions." Cold Spring Harb Perspect Biol **1**(1): a002576.

Harris, A. L. (2001). "Emerging issues of connexin channels: biophysics fills the gap." Q Rev Biophys **34**(3): 325-472.

Herve, J. C. and M. Derangeon (2013). "Gap-junction-mediated cell-to-cell communication." Cell Tissue Res **352**(1): 21-31.

Hoshi, T., W. N. Zagotta, et al. (1990). "Biophysical and molecular mechanisms of Shaker potassium channel inactivation." Science **250**(4980): 533-538.

Hu, X. and G. Dahl (1999). "Exchange of conductance and gating properties between gap junction hemichannels." FEBS Lett **451**(2): 113-117.

Hu, X., M. Ma, et al. (2006). "Conductance of connexin hemichannels segregates with the first transmembrane segment." Biophys J **90**(1): 140-150.

Kronengold, J., E. B. Trexler, et al. (2003). "Single-channel SCAM identifies pore-lining residues in the first extracellular loop and first transmembrane domains of Cx46 hemichannels." J Gen Physiol **122**(4): 389-405.

Kwak, B. R., J. C. Saez, et al. (1995). "Effects of cGMP-dependent phosphorylation on rat and human connexin43 gap junction channels." Pflugers Arch **430**(5): 770-778.

Lazrak, A. and C. Peracchia (1993). "Gap junction gating sensitivity to physiological internal calcium regardless of pH in Novikoff hepatoma cells." Biophys J **65**(5): 2002-2012.

Lin, J. S., R. Eckert, et al. (1998). "Spatial differences in gap junction gating in the lens are a consequence of connexin cleavage." Eur J Cell Biol **76**(4): 246-250.

Loewenstein, W. R. (1981). "Junctional intercellular communication: the cell-to-cell membrane channel." Physiol Rev **61**(4): 829-913.

Maeda, S., S. Nakagawa, et al. (2009). "Structure of the connexin 26 gap junction channel at 3.5A resolution." Nature **458**(7238): 597-602.

Maeda, S. and T. Tsukihara (2011). "Structure of the gap junction channel and its implications for its biological functions." Cell Mol Life Sci **68**(7): 1115-1129.

Mathias, R. T., T. W. White, et al. (2010). "Lens gap junctions in growth, differentiation, and homeostasis." Physiol Rev **90**(1): 179-206.

Mese, G., C. Sellitto, et al. (2011). "The Cx26-G45E mutation displays increased hemichannel activity in a mouse model of the lethal form of keratitis-ichthyosis-deafness syndrome." Mol Biol Cell **22**(24): 4776-4786.

Milks, L. C., N. M. Kumar, et al. (1988). "Topology of the 32-kd liver gap junction protein determined by site-directed antibody localizations." EMBO J **7**(10): 2967-2975.

Moreno, A. P., M. Chanson, et al. (2002). "Role of the carboxyl terminal of connexin43 in transjunctional fast voltage gating." Circ Res **90**(4): 450-457.

Moreno, A. P., J. G. Laing, et al. (1995). "Properties of gap junction channels formed of connexin 45 endogenously expressed in human hepatoma (SKHep1) cells." Am J Physiol **268**(2 Pt 1): C356-365.

Moreno, A. P., J. C. Saez, et al. (1994). "Human connexin43 gap junction channels. Regulation of unitary conductances by phosphorylation." Circ Res **74**(6): 1050-1057.

Nakagawa, S., S. Maeda, et al. (2010). "Structural and functional studies of gap junction channels." Curr Opin Struct Biol **20**(4): 423-430.

Oh, S., C. K. Abrams, et al. (2000). "Stoichiometry of transjunctional voltage-gating polarity reversal by a negative charge substitution in the amino terminus of a connexin32 chimera." J Gen Physiol **116**(1): 13-31.

Oh, S., S. Rivkin, et al. (2004). "Determinants of gating polarity of a connexin 32 hemichannel." Biophys J **87**(2): 912-928.

Oh, S., J. B. Rubin, et al. (1999). "Molecular determinants of electrical rectification of single channel conductance in gap junctions formed by connexins 26 and 32." J Gen Physiol **114**(3): 339-364.

Paul, D. L., L. Ebihara, et al. (1991). "Connexin46, a novel lens gap junction protein, induces voltage-gated currents in nonjunctional plasma membrane of Xenopus oocytes." J Cell Biol **115**(4): 1077-1089.

Paulauskas, N., M. Pranevicius, et al. (2009). "A stochastic four-state model of contingent gating of gap junction channels containing two "fast" gates sensitive to transjunctional voltage." Biophys J **96**(10): 3936-3948.

Peracchia, C., G. Bernardini, et al. (1983). "Is calmodulin involved in the regulation of gap junction permeability?" Pflugers Arch **399**(2): 152-154.

Peracchia, C. and L. L. Peracchia (2005). "Inversion of both gating polarity and CO2 sensitivity of voltage gating with D3N mutation of Cx50." Am J Physiol Cell Physiol **288**(6): C1381-1389.

Rackauskas, M., M. M. Kreuzberg, et al. (2007). "Gating properties of heterotypic gap junction channels formed of connexins 40, 43, and 45." Biophys J **92**(6): 1952-1965.

Revilla, A., M. V. Bennett, et al. (2000). "Molecular determinants of membrane potential dependence in vertebrate gap junction channels." Proc Natl Acad Sci U S A **97**(26): 14760-14765.

Revilla, A., C. Castro, et al. (1999). "Molecular dissection of transjunctional voltage dependence in the connexin-32 and connexin-43 junctions." Biophys J **77**(3): 1374-1383.

Ri, Y., J. A. Ballesteros, et al. (1999). "The role of a conserved proline residue in mediating conformational changes associated with voltage gating of Cx32 gap junctions." Biophys J **76**(6): 2887-2898.

Rong, P., X. Wang, et al. (2002). "Disruption of Gja8 (alpha8 connexin) in mice leads to microphthalmia associated with retardation of lens growth and lens fiber maturation." Development **129**(1): 167-174.

Sankararamakrishnan, R. and S. Vishveshwara (1992). "Geometry of proline-containing alpha-helices in proteins." Int J Pept Protein Res **39**(4):

356-363.

Sellitto, C., L. Li, et al. (2004). "Connexin50 is essential for normal postnatal lens cell proliferation." Invest Ophthalmol Vis Sci **45**(9): 3196-3202.

Shibayama, J., C. Gutierrez, et al. (2006). "Effect of charge substitutions at residue his-142 on voltage gating of connexin43 channels." Biophys J **91**(11): 4054-4063.

Srinivas, M., D. P. Calderon, et al. (2006). "Regulation of connexin hemichannels by monovalent cations." J Gen Physiol **127**(1): 67-75.

Srinivas, M., M. Costa, et al. (1999). "Voltage dependence of macroscopic and unitary currents of gap junction channels formed by mouse connexin50 expressed in rat neuroblastoma cells." J Physiol **517 ( Pt 3)**: 673-689.

Srinivas, M., J. Kronengold, et al. (2005). "Correlative studies of gating in Cx46 and Cx50 hemichannels and gap junction channels." Biophys J **88**(3): 1725-1739.

Suchyna, T. M., J. M. Nitsche, et al. (1999). "Different ionic selectivities for connexins 26 and 32 produce rectifying gap junction channels." Biophys J **77**(6): 2968-2987.

Suchyna, T. M., L. X. Xu, et al. (1993). "Identification of a proline residue as a transduction element involved in voltage gating of gap junctions." Nature **365**(6449): 847-849.

Sun, W., X. Xiao, et al. (2011). "Mutational screening of six genes in Chinese patients with congenital cataract and microcornea." Mol Vis **17**: 1508-1513.

Sun, Y., M. D. Hills, et al. (2014). "Atrial Fibrillation-Linked Germline GJA5/Connexin40 Mutants Showed an Increased Hemichannel Function." PLoS One **9**(4): e95125.

Tang, Q., T. L. Dowd, et al. (2009). "Conformational changes in a pore-forming region underlie voltage-dependent "loop gating" of an unapposed connexin hemichannel." J Gen Physiol **133**(6): 555-570.

Tong, J. J., X. Liu, et al. (2004). "Exchange of gating properties between rat cx46 and chicken cx45.6." Biophys J **87**(4): 2397-2406.

Tong, J. J., P. J. Minogue, et al. (2011). "Different consequences of cataract-associated mutations at adjacent positions in the first extracellular boundary of connexin50." Am J Physiol Cell Physiol **300**(5): C1055-1064.

Trexler, E. B., M. V. Bennett, et al. (1996). "Voltage gating and permeation in a gap junction hemichannel." Proc Natl Acad Sci U S A **93**(12): 5836-5841.

Trexler, E. B., F. F. Bukauskas, et al. (1999). "Rapid and direct effects of pH on connexins revealed by the connexin46 hemichannel preparation." J Gen Physiol **113**(5): 721-742.

Trexler, E. B., F. F. Bukauskas, et al. (2000). "The first extracellular loop domain is a major determinant of charge selectivity in connexin46 channels." Biophys J **79**(6): 3036-3051.

Valiunas, V., D. Manthey, et al. (1999). "Biophysical properties of mouse connexin30 gap junction channels studied in transfected human HeLa cells." J Physiol **519 Pt 3**: 631-644.

Verselis, V. K., C. S. Ginter, et al. (1994). "Opposite voltage gating polarities of two

closely related connexins." <u>Nature</u> **368**(6469): 348-351.

Verselis, V. K., M. P. Trelles, et al. (2009). "Loop gating of connexin hemichannels involves movement of pore-lining residues in the first extracellular loop domain." <u>J Biol Chem</u> **284**(7): 4484-4493.

Verselis, V. K., E. B. Trexler, et al. (2000). "Connexin hemichannels and cell-cell channels: comparison of properties." <u>Braz J Med Biol Res</u> **33**(4): 379-389.

White, T. W., R. Bruzzone, et al. (1992). "Mouse Cx50, a functional member of the connexin family of gap junction proteins, is the lens fiber protein MP70." <u>Mol Biol Cell</u> **3**(7): 711-720.

White, T. W., D. A. Goodenough, et al. (1998). "Targeted ablation of connexin50 in mice results in microphthalmia and zonular pulverulent cataracts." <u>J Cell Biol</u> **143**(3): 815-825.

Xin, L., X. Q. Gong, et al. (2010). "The role of amino terminus of mouse Cx50 in determining transjunctional voltage-dependent gating and unitary conductance." <u>Biophys J</u> **99**(7): 2077-2086.

Xin, L., S. Nakagawa, et al. (2012). "Aspartic acid residue D3 critically determines Cx50 gap junction channel transjunctional voltage-dependent gating and unitary conductance." <u>Biophys J</u> **102**(5): 1022-1031.

Zhou, Y., W. Yang, et al. (2007). "Identification of the calmodulin binding domain of connexin 43." <u>J Biol Chem</u> **282**(48): 35005-35017.

# Chapter 2: Article

## Charge at the 46th residue of Cx50 is critical for gap junctional unitary conductance and transjunctional voltage-dependent gating

Xiaoling Tong,[1] Hiroshi Aoyama, [2] Tomitake Tsukihara[3,4] and Donglin Bai[1]

[1]Department of Physiology and Pharmacology, University of Western Ontario, London, Ontario, Canada

[2]Graduate School of Pharmaceutical Sciences, Osaka University, Osaka, Japan

[3]Institutes for Protein Research, Osaka University, Osaka, Japan

[4]Department of Life Science, University of Hyogo, 3-2-1 Koto, Kamighori, Akoh, Hyogo 678-1297, Japan

## 2.1 Chapter summary

Gap junction (GJ) channels are twice the length of most membrane channels, yet they often have large unitary conductance ($\gamma_j$). What factors make this possibly the longest channel so efficient in passing ions are not fully clear. Here we studied the lens Cx50 GJ channels, which display one of the largest $\gamma_j$ and the most sensitive transjunctional voltage-dependent gating ($V_j$-gating) among all GJ channels. Introduction of charged residues into a putative pore lining domain 'TM1/E1 border' (the border of the first transmembrane domain and the first extracellular loop) drastically altered the $\gamma_j$. Specifically G46D and G46E increased the Cx50 $\gamma_j$ from 201 to 256 and 293 pS, respectively, and the G46K channel showed an $\gamma_j$ of only 20 pS. G46K also drastically altered $V_j$-gating properties in homotypic G46K and heterotypic Cx50/G46K channels, causing a loss of fast $V_j$-dependent gating transitions and leaving only loop gating transitions in the single channel current recordings. In addition, both macroscopic and single channel currents of heterotypic Cx50/G46K channels showed a prominent rectification. The homology structural models of Cx50 GJ channel and its mutants indicate that the pore surface electrostatic potential at the TM1/E1 border is a dictating factor in determining $\gamma_j$ and $V_j$-gating probably by regulating the efficiency of ion permeation through this particular section.

## 2.2   Introduction

Gap junction (GJ) channels allow direct intercellular exchange of ions and small signaling/metabolic molecules between neighboring cells and play a key role in many physiological processes (Saez *et al.*, 2003; Goodenough & Paul, 2009). GJ channels are oligomeric connexins of 21 different members (Sohl & Willecke, 2004; Goodenough & Paul, 2009), all of which with similar structural topology, including four transmembrane domains (TM1 to TM4), two extracellular loops (E1 and E2), one cytoplasmic loop (CL), with the placement of both amino terminus (NT) and carboxyl terminus (CT) in the cytosol (Simon & Goodenough, 1998; Saez *et al.*, 2003; Sohl & Willecke, 2004). Six connexin molecules oligomerize to form a hemichannel and two hemichannels dock together at their extracellular domains to construct a whole GJ channel (a dodecamer of connexins). This unique structural arrangement of GJ channels makes them twice as long as most of the membrane channels and has probably the longest permeation passage for any membrane channels, yet the single channel conductance ($\gamma_j$) of a GJ channel can be as high as hundreds of picoSiemens (pS) in several homotypic GJs (Reed *et al.*, 1993; Veenstra *et al.*, 1994; Bukauskas *et al.*, 1995; Srinivas *et al.*, 1999). What makes the GJ channel so efficient in passing ions is not fully clear. One classical hypothesis believes that the pore diameter of a GJ channel docked by two hexameric hemichannels is much larger than those tetrameric or pentameric membrane channels, which facilitates rapid ion permeation through the GJ channel (Hille, 2001). It is true that most GJ channels have a larger pore, allowing not only ions, but also other signaling/metabolic molecules up to 1 kDa to pass

through. However, this model is unable to explain the well-documented experimental data that several GJ channels with large $\gamma_j$s showed a much lower cut off size on permeable molecules than those GJ channels with much lower $\gamma_j$s (Veenstra *et al.*, 1995; Gong & Nicholson, 2001; Weber *et al.*, 2004; Ek-Vitorin & Burt, 2005; Dong *et al.*, 2006), indicating that other pore properties also play an important role in facilitating ion permeation. Experimental evidence is accumulated largely from hemichannel studies that the TM1/E1 border likely forms part of the channel inner surface and plays a key role in determining the channel conductance of several connexins (Kronengold *et al.*, 2003; Tang *et al.*, 2009; Verselis *et al.*, 2009), including Cx26 (Verselis *et al.*, 1994; Sanchez *et al.*, 2010; Sanchez *et al.*, 2013). This structural prediction was confirmed by the high resolution (at 3.5 Å) crystal structure of Cx26 GJ channel (Maeda *et al.*, 2009). The amino acid residues at the TM1/E1 border form a narrow passage of the pore with a specialized helical structure [called 3(10) or parahelix for the residues of 42 - 51], which exposes several acidic residues toward the pore lumen to form a negatively charged pathway. Two such negatively charge-enriched pathways in each Cx26 GJ channel are believed to increase local cation concentration and facilitate the rate of cation permeation (Maeda *et al.*, 2009). Several connexins, including Cx50, show high sequence identity and homology with Cx26, especially at the TM1/E1 border domain, arguing that their GJ channels might have a similar overall structure, as well as the negatively charged pathway, which could be associated with the experimentally observed cation preference (Srinivas *et al.*, 1999).

To study the function of TM1/E1 border domain in Cx50 channel $\gamma_j$ and $V_j$-gating properties, we generated mutants with an additional negatively or positively charged residue in this domain (G46D/E and G46K). These mutations are predicted to decrease the pore size and alter the surface electrostatic potentials in the negatively charged pathway because of the pore-lining position of G46. Both G46D and G46E channels showed significantly increased $\gamma_j$, while G46K channels substantially reduced the apparent $\gamma_j$. No fast gating and only loop gating was observed in G46K GJ channels. Our homology models indicate that the surface electrostatic property at the TM1/E1 border of Cx50 GJ channel rather than the local pore size is more important in determining the rate of ion permeation, which would further influence $\gamma_j$ and $V_j$-gating properties of GJ channels.

## 2.3 Materials and methods

### 2.3.1 Construction of Cx50 mutants

Mouse Cx50 cDNA was carried in the pIRES2-EGFP vector and this construct was used as the template for the point mutants, G46D, G46E and G46K. The Quick-Change site directed mutagenesis kit (Stratagene, La Jolla, CA) was used to generate the mutants with following primers:

G46D   Forward: 5' GGAGTTTGTGTGGGACGATGAGCAATC 3'

         Reverse: 5' GATTGCTCATCGTCCCACACAAACTCC 3'

G46E   Forward: 5' GCGGAGTTTGTGTGGGAGGATGAGCAATCTG 3'

         Reverse: 5' CAGATTGCTCATCCTCCCACACAAACTCCGC 3'

G46K   Forward: 5' GCGGAGTTTGTGTGGAAGGATGAGCAATCTG 3'

         Reverse: 5' CAGATTGCTCATCCTTCCACACAAACTCCGC 3'

### 2.3.2 Cell culture and transient transfection

Mouse neuroblastoma (N2A) cells were purchased from American Type Culture Collection (ATCC, Manassas, VA) and cultured with Dulbecco's modified Eagle's medium containing 10% fetal bovine serum (FBS). Before transfection, cells were plated in 35 mm dishes and the confluence was around 50% after overnight culture. 1.5 μg Cx50 construct or mutant vector was transfected with 2 μl X-tremeGENE HP DNA Transfection Reagent (Roche Applied Sciences, Indianapolis, IN). Cells were cultured for 24 hours after transfection and replated on to glass coverslips ~1-3 hours prior patch clamping recording.

29

When studying heterotypic Cx50/G46K GJs, Cx50 cDNA was carried in pcDNA3.1(-) expression vector and cotransfected with DsRed cDNA at a ratio of 4:1. G46K-IRES-GFP vector was transfected separately and the transfected cells were mixed with Cx50 and DsRed expressing cells to obtain heterotypic cell pairs. Only red/green cell pairs were chosen for patch clamp recording.

### 2.3.3 Electrophysiological recording

The $V_j$-gating property of cell pairs expressing either Cx50 or its mutants was measured by dual whole-cell voltage-clamp technique as described earlier (Bai *et al.*, 2006; Xin *et al.*, 2010). Transfected cells were replated on glass coverslips with appropriate cell density for ~1-3 hours, and then transferred to a recording chamber on an inverted microscope (Leica DM IRB), bathed in extracellular fluid (ECF) at room temperature. The composition of ECF is (in mM): 140 NaCl, 2 CsCl, 2 CaCl$_2$, 1 MgCl$_2$, 5 Hepes, 4 KCl, 5 D-glucose, 2 Pyruvate, pH 7.2. Paired GFP-positive cells were patched by two glass micropipettes (pipette resistance 2 - 5 MΩ) which were filled with intracellular fluid (ICF) containing (in mM): 130 CsCl, 10 EGTA, 0.5 CaCl$_2$, 3 MgATP, 2 Na$_2$ATP, 10 Hepes, pH 7.2. Isolated cell pairs were selected and both of them were voltage clamped at 0 mV. The common protocol was that one cell of the pair was clamped at 0 mV while the apposed cell was administrated with a series of voltage pulses from $\pm$ 20 mV to $\pm$ 100 mV in 20 mV increments with 7 seconds duration. The junctional currents (I$_j$s) were amplified with two Axopatch 200B amplifiers with a low-pass filter (cut-off frequency 1 kHz) and digitalized at 10 kHz sampling rate via an ADDA converter (Digidata 1322A, Molecular devices, Sunnyvale, CA).

For the ion preference experiment, the principal electrolyte in the ICF, CsCl, was

replaced by equimolar concentration of tetraethylammonium chloride (TEACl) to eliminate/reduce the cation current (due to a much bulkier size of $TEA^+$ than $Cs^+$), or cesium glutamate (CsGlu) to diminish/reduce anion current (as $Glu^-$ is much larger than $Cl^-$). CsGlu solution was prepared by mixing the same molar CsOH with glutamic acid solution.

### 2.3.4    Homology structure modeling

The sequence of mouse Cx50 was aligned with that of Cx26 for the homology structure model. High sequence identity is observed in these two proteins (overall 49% and on the structure resolved part 57%). Cx26 crystal structure (2WZ3) (Maeda *et al.*, 2009) was used as a template to replace residue by residue for the Cx50 structure. When a Cx50 residue replacement in the structure caused an abnormal inter-atomic contact, this was adjusted by hand initially in COOT and then revised by CNS energy refinement. After the energy refinement, structural validity of the model was inspected manually as described earlier (Nakagawa *et al.*, 2011; Gong *et al.*, 2013). Adaptive Poisson-Boltzman Solver (APBS) (Baker *et al.*, 2001) and PDB2PQR server (http://nbcr-222.ucsd.edu/pdb2pqr_1.8/) were used to calculate the electron potentials of all atoms in the protein. The APBS parameters were set as described previously (Maeda *et al.*, 2009). PyMOL program was used for the diameter measurements and the structure presentations (DeLano, 2006).

### 2.3.5    Data analysis

To minimize the influence of series resistance on $V_j$-gating properties, only those cell pairs with $\leq 5$ nS junctional conductance ($G_j$) were selected for Boltzmann fitting analysis (Wilders & Jongsma, 1992). For each current trace, the normalized

steady-state conductance ($G_{j,ss}$) was obtained by normalizing the steady state current to the peak current. The dependence of $G_{j,ss}$ on positive and negative $V_j$ was plotted and fitted with a two-state Boltzmann equation independently:

$$G_{j,ss} = (G_{max} - G_{min})/ \{1 + exp[A(V_j - V_0)]\} + G_{min}$$

$V_0$ is the voltage at which the conductance is reduced by half [$(G_{max} - G_{min})/2$]; $G_{max}$ is the maximum normalized conductance; $G_{min}$ is the normalized voltage-insensitive residual conductance, and parameter $A$, which describes the slope of the fitted curve, reflects the $V_j$ sensitivity of the GJ channels.

To record single channel current, cell pairs with one or two operational channels were obtained by shortening the expression time after transfection. The amplitudes of $i_j$s were measured directly using Clampfit9 after digital filtering and plotted to corresponding $V_j$s. The $i_j$-$V_j$ plot was fitted by linear regression through the origin of the coordinates. The slope of the linear regression line is defined as the slope unitary conductance ($\gamma_j$).

The open ($P_o$), subconductance ($P_s$) or close ($P_c$) probability represents the fraction of time that the channel resides in open, subconductance or close state, respectively. To quantitatively measure the $P_o$, $P_s$ and $P_c$ in Cx50 and G46D channels, the amplitudes of single channel currents during each $V_j$ pulse were binned into all-point histograms to obtain the number of data points for each category (including open / subconductance / close state) separately, which was then divided by the total number of points.

To analyze single channel open dwell time, the single channel current records were digitally filtered at 500 Hz (Gaussian) and any events reaching half amplitude height and lasting >2 ms were considered as open events. The open events at the

beginning and end of $V_j$ pulse were discarded as the duration of these events were likely to be cut short by the $V_j$ pulse. The dwell times of analyzed events were binned into histograms and were fitted with two exponentials with time constants, $\tau_1$ and $\tau_2$, as described previously (Xin *et al.*, 2010). $\tau_{mean}$ was calculated from the sum of individual time constant with its weight.

## 2.4　Results

### 2.4.1　G46D formed functional GJ channels with similar $V_j$-gating properties as those of Cx50

G46D was generated to increase the negative electrostatic surface potential in the middle of the TM1/E1 border of the GJ channel. Macroscopic transjunctional currents ($I_j$s) in cell pairs expressing either Cx50 or G46D were obtained in response to the $V_j$ pulses shown in Fig. 2.1A. The $I_j$ of G46D-expressing cell pairs showed symmetrical $V_j$-dependent inactivation when the absolute value of $V_j$ was $\geq 40$ mV. Normalized steady state junctional conductance ($G_{j,ss}$) values from 6 cell pairs expressing either Cx50 or G46D were plotted against corresponding $V_j$s and their Boltzmann fitted curves are almost identical to each other (Fig. 2.1B and Table 2.1), indicating that G46D has little changes in the macroscopic $V_j$-gating properties.
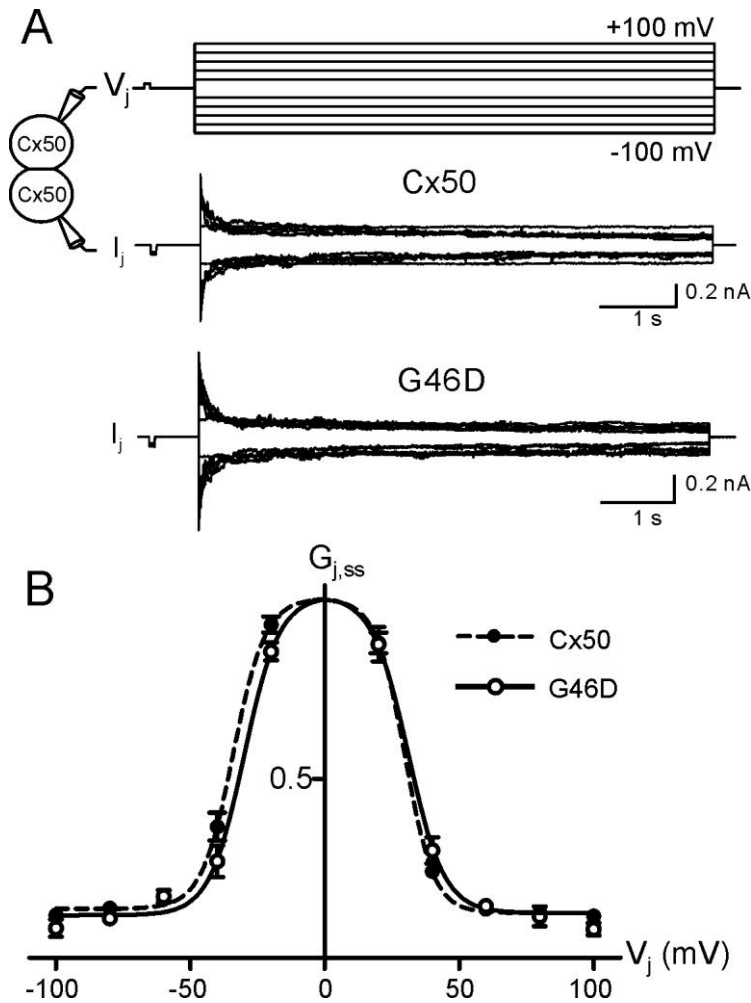
**Fig 2.1  Macroscopic $V_j$-gating properties of Cx50 and G46D GJ channels. A)** $V_j$ pulses from $\pm 20$ mV to $\pm 100$ mV in 20 mV increments were applied to one cell of the cell pair expressing Cx50 or G46D and macroscopic transjunctional currents ($I_j$s) recorded from the other cell are presented. **B)** Normalized $G_{j,ss}$ of Cx50 (solid circles) and G46D (open circles) were plotted against different $V_j$s. The smooth dash and solid lines represent the best fitting curves of the averaged data from Cx50 (n = 6) and G46D (n = 6) channels to a two-state Boltzmann function.

**Table 2.1    Boltzmann fitting parameters for Cx50 and its mutants**

| | $V_j$ polarity | $G_{min}$ | $V_0$ | $A$ |
|---|---|---|---|---|
| Cx50 | + | $0.13 \pm 0.01$ | $29.8 \pm 0.8$ | $0.18 \pm 0.01$ |
| | − | $0.14 \pm 0.01$ | $33.6 \pm 1.0$ | $0.16 \pm 0.02$ |
| G46D | + | $0.13 \pm 0.02$ | $31.1 \pm 1.5$ | $0.15 \pm 0.02^{**}$ |
| | − | $0.12 \pm 0.02$ | $30.0 \pm 1.2^{***}$ | $0.15 \pm 0.02$ |
| G46E | + | $0.11 \pm 0.01^{**}$ | $28.1 \pm 0.8^{**}$ | $0.17 \pm 0.01$ |
| | − | $0.11 \pm 0.01^{***}$ | $28.8 \pm 0.8^{***}$ | $0.19 \pm 0.02^{*}$ |
| G46K | + | $0.55 \pm 0.09^{***}$ | $50.7 \pm 10.4^{***}$ | $0.05 \pm 0.04^{***}$ |
| | − | $0.60 \pm 0.06^{***}$ | $53.4 \pm 6.9^{***}$ | $0.05 \pm 0.02^{***}$ |
| Cx50/G46K | + | $0.07 \pm 0.14$ | $28.1 \pm 17.5$ | $0.04 \pm 0.02^{***}$ |
| | − | — | — | — |

Data are presented as mean $\pm$ SEM and $V_0$ are absolute values. Student's *t*-test was used to compare the Boltzmann fitting parameters of the mutants against those of the wild-type Cx50 with the same $V_j$ polarity. Asterisks indicate the statistical difference (* $p < 0.05$, ** $p < 0.01$, *** $p < 0.001$).

## 2.4.2  G46D increased $\gamma_j$ and the probability of fully closed state, but decreased open dwell time

The single channel current ($i_j$) records of Cx50 and G46D GJs were obtained from cell pairs coupled with only one operational channel (Fig. 2.2A right panel). The G46D channel properties are different from those of Cx50 channels. First, the $\gamma_j$ of G46D channel, estimated from a linear regression of $i_j$-$V_j$ plots (Fig. 2.2A, B), was significantly increased to $256 \pm 5$ pS (n = 8) comparing to Cx50 $\gamma_j$ ($201 \pm 2$ pS, n = 8, p < 0.001). Second, at the $V_j$s of $\pm 60$ to $\pm 80$ mV, Cx50 channels usually showed few open events at the initial $V_j$ pulses (Fig. 2.2A). Then, the channel dwelled almost exclusively at a subconductance state (Fig. 2.2A left panel) and occasionally showed brief entries into the fully closed state (Fig. 2.2A left panel arrow). Similar to Cx50, the main open events of G46D channel usually clustered in the initial part of $i_j$ recording. The subconductance states were also observed, but often with intermittent long-lived fully closed states (Fig. 2.2A, right panel arrows). To quantify this observation, the probability of open ($P_o$), closed ($P_c$) and subconductance ($P_s$) states were measured and plotted to $V_j$s of $\pm 60$ and $\pm 80$ mV (Fig. 2.2C). The most significant changes of G46D channel were the elevation of $P_c$, with a concurrent decrease in $P_s$ ($V_j \pm 80$ mV) or an apparent decrease of both $P_o$ and $P_s$ ($V_j \pm 60$ mV). The significant increase in the $P_c$ in G46D channels is probably due to an increased occurrence of loop gating, an increased stability of fully closed state or the combinations of both factors. Finally, as shown in Fig. 2.2A, the open dwell time for G46D channel appeared to be shorter than that of Cx50. This was measured

37

systematically at several $V_j$s (Fig. 2.2D). At these $V_j$s for both G46D and Cx50, the open dwell times displayed two time constants ($\tau_1$ and $\tau_2$) with various distributions. The weighted average open dwell time ($\tau_{mean}$) for G46D was getting shorter with the increase in $V_j$ values from $\pm 40$ mV (77 ms), $\pm 60$ mV (44 ms) to $\pm 80$ mV (19 ms). At all $V_j$s, the $\tau_{mean}$s of G46D channel were shorter than those corresponding ones of Cx50 (Fig. 2.2D), indicating that the open state of G46D channel is less stable and easier to transfer to a subconductance or fully closed state at these $V_j$s.

**A**

Cx50                                          G46D

$+V_j$
0                          $V_j$        0                          $-V_j$

±20

±40

±60

+80
(mV)

10 pA

1 s

**B**

$i_j$ (pA)

G46D (256 pS)

Cx50 (201 pS)

$V_j$ (mV)

**C**

Probability

☐ Cx50
■ G46D

**          **

*

$P_o$   $P_s$   $P_c$        $P_o$   $P_s$   $P_c$

± 60 mV              ± 80 mV

**D**

± 40 mV                    ± 60 mV                    ± 80mV

Square root count (N)

$\tau_1$=58 ms (42%)    $\tau_2$=259 ms (58%)    $\tau_1$=37 ms (36%)    $\tau_2$=147 ms (64%)    $\tau_1$=20 ms (47%)    $\tau_2$=111 ms (53%)

$\tau_{mean}$=175 ms          $\tau_{mean}$=107 ms          $\tau_{mean}$=68 ms          Cx50

$\tau_1$=16 ms (31%)    $\tau_2$=105 ms (69%)    $\tau_1$=9 ms (30%)    $\tau_2$=59 ms (70%)    $\tau_1$=9 ms (80%)    $\tau_2$=57 ms (20%)

$\tau_{mean}$=77 ms          $\tau_{mean}$=44 ms          $\tau_{mean}$=19 ms          G46D
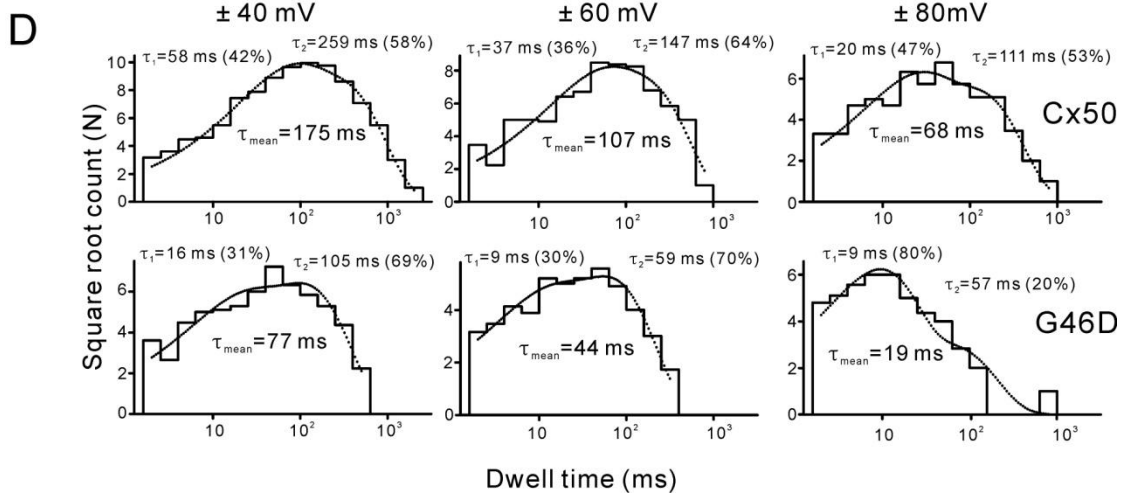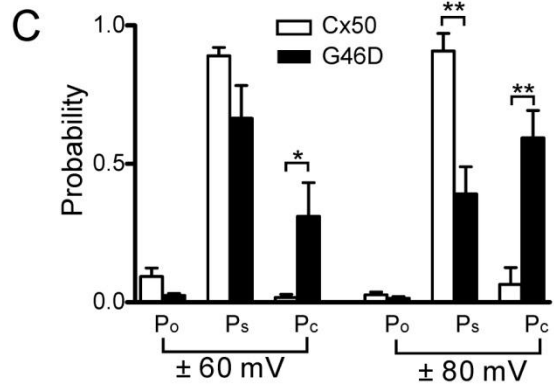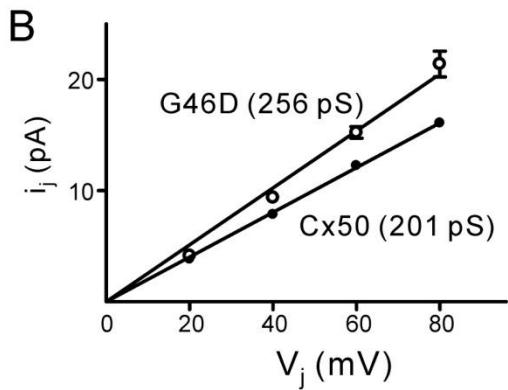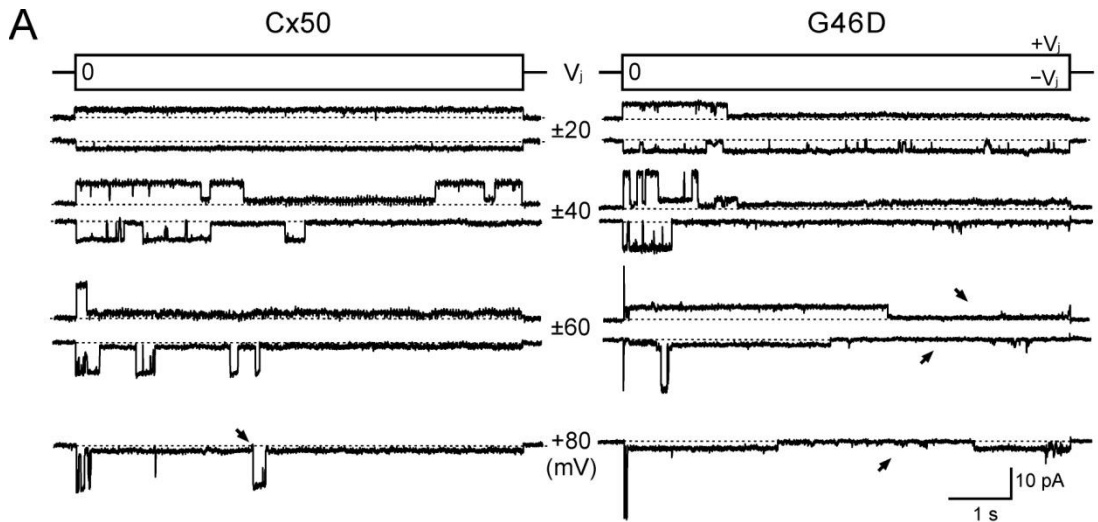
Dwell time (ms)

39

**Fig. 2.2   G46D alters single channel properties. A)** Representative single channel

current records of Cx50 channel (left) and G46D channel (right) are illustrated in

response to different $V_j$s as indicated. Single channel currents of G46D displayed a

shortened dwell time of most open events at different $V_j$s and long-lived fully closed

state (pointed by arrows on the right panel) in response to $\pm 60$ mV and $+ 80$ mV

pulses. A brief transition to fully closed state is indicated in Cx50 channel (arrow on

the left panel). The dotted lines indicate the fully closed current level. **B)** Average

single channel slope conductance ($\gamma_j$) of G46D channel (n = 8) was much higher than

that of Cx50 (n = 8, p < 0.001). **C)** $P_o$, $P_s$ and $P_c$ represent the probabilities of the

channel in open, subconductance and fully closed state, respectively. Bar graph

illustrates the average data from 4 different cell pairs. Asterisks above the bar

indicates statistical difference (* p < 0.05, ** p < 0.01). G46D channel demonstrated a

markedly increased $P_c$ at these $V_j$s. **D)** The open dwell time of G46D channel is

shorter than that of Cx50. The dotted lines are the Gaussian fit of a two-term

exponential function to the histograms. The time constants $\tau_1$ and $\tau_2$ with their relative

weight are shown. $\tau_{mean}$ is the mean open dwell time obtained from the sum of the

product of each $\tau$ and its relative weight. $\tau_1$, $\tau_2$ and $\tau_{mean}$ are all reduced in G46D

channel.

### 2.4.3 G46E channel showed higher $\gamma_j$ than that of G46D

Increased $\gamma_j$ of G46D channel is surprising because the side chain of Asp (D) is much larger than that of Gly (G). G46D mutation is predicted to decrease physical pore size at the $46^{th}$ position. However, introduction of a negatively charged residue might alter the local pore surface electrostatic properties, which could facilitate the ion permeation through this cation-preferring channel (Srinivas *et al.*, 1999). To further test this hypothesis, we generated another mutant, G46E, in which Gly (G) was replaced by another negatively charged residue Glu (E) with a longer side chain than Asp (D). As shown in Fig. 2.3A, macroscopic $I_j$s in response to the same $V_j$ pulses were similar to those observed in Cx50 channels. $G_{j,ss}$-$V_j$ plots of G46E channel were well fitted by the Boltzmann equation at both $V_j$ polarities and the fitted curves are virtually identical to those of Cx50 (Table 2.1).

At single channel level, the $\gamma_j$ of G46E channel, generated by $i_j$-$V_j$ plot, was 293 $\pm 4$ pS (n = 4), nearly 50% larger than that of Cx50 (Fig. 2.3B). It is also significantly larger than that of G46D (p < 0.001). The $i_j$s showed long-lived fully closed state at the tested $V_j$s (Fig. 2.3C, arrows), similar to those observed in G46D channels. A temporal expansion of a cluster of open events at 80 mV $V_j$ indicates that G46E channel also showed a shorter open dwell time (all of the open events are shorter than 40 ms) than that of Cx50 channel (with a $\tau_{mean} = 68$ ms at this $V_j$). In summary, the characteristics of G46E channel seem to resemble those of G46D at both macroscopic and single channel levels. The only exception is that G46E produced an even larger $\gamma_j$ than G46D.
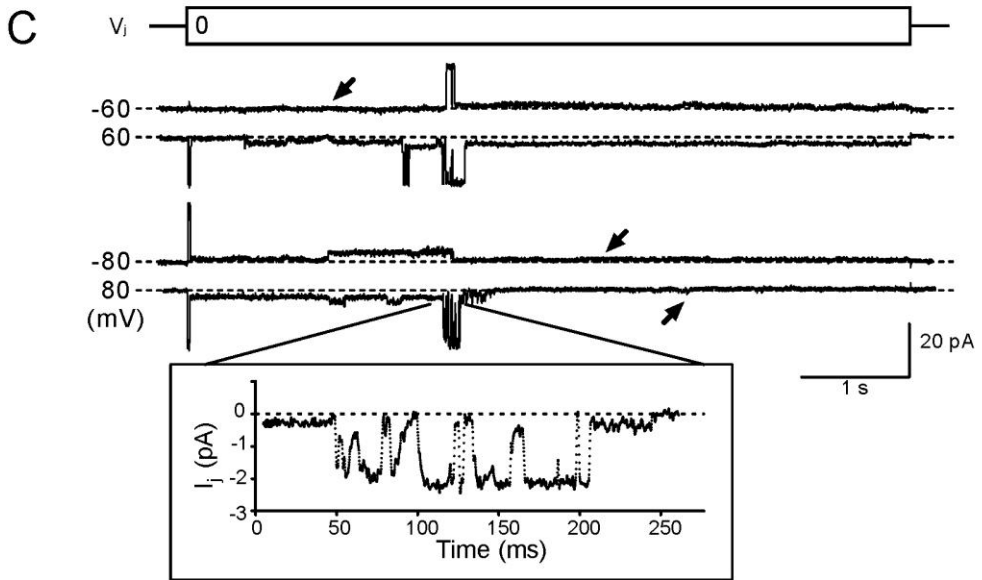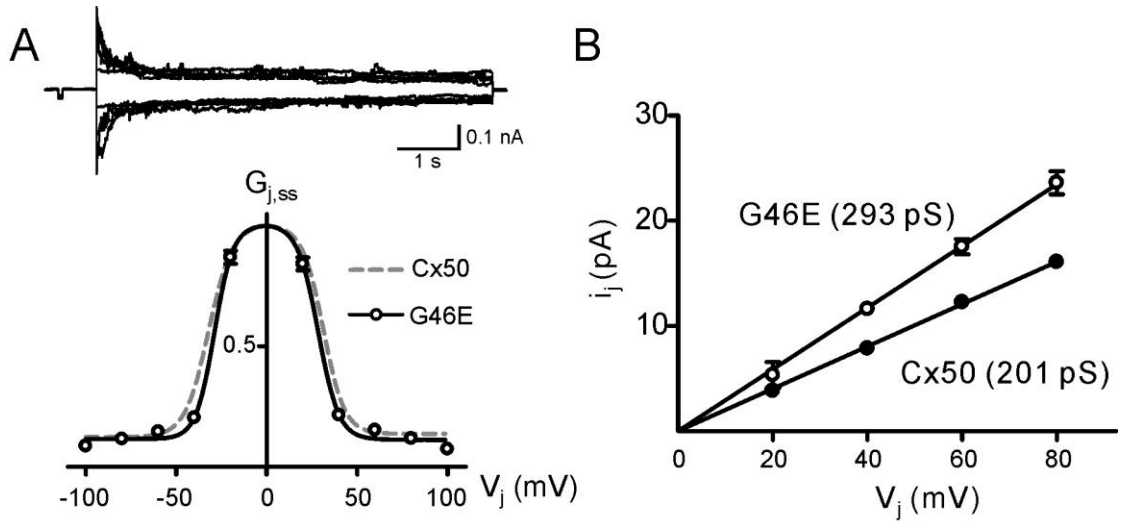
**Fig. 2.3** **Macroscopic and single channel properties of G46E GJs. A)** Macroscopic junctional currents ($I_j$s) of homotypic G46E channels are shown in response to the same $V_j$s as shown in Fig. 2.1A. $G_{j,ss}$-$V_j$ relationships of G46D were constructed (n = 6) and were fitted to Boltzmann functions. The fitting curves of Cx50 (grey dashed lines) are obtained from Fig. 2.1B for comparison. **B)** Linear regression of $i_j$-$V_j$ plots showed an increased $\gamma_j$ of G46E channel (n = 4, p < 0.001 vs Cx50 [same as shown in Fig. 2.2B]). **C)** Single channel current traces of G46E channel under the indicated $V_j$s showed the existence of main open state, subconductance state and fully closed state. Arrows point to the long-lived fully closed state. Temporal expanded trace (inset) with multiple openings indicates the open dwell times in these open events were short.

### 2.4.4   G46K channels showed much lower $\gamma_j$ and an altered $V_j$-gating

Introduction of a negatively charged residue at the TM1/E1 border (mutants G46D/E) drastically increased $\gamma_j$. To explore the effects of introducing a positively charged residue into this domain, G46K was generated. Different from those of Cx50, the $I_j$s of G46K channel showed little $V_j$-dependent inactivation in the range of $\pm 40$ mV, while larger $V_j$ pulses ($\pm 60$ to $\pm 100$ mV) only produced a moderate level of inactivation (Fig. 2.4A). The $G_{j,ss}$-$V_j$ plot and the associated Boltzmann fitting curves of G46K channels were drastically different from those of Cx50 (Fig. 2.4B). Multiple Boltzmann fitting parameters of G46K channel were different from Cx50 channel, including larger $G_{min}$s and decreased $V_j$-gating sensitivities (Table 2.1).

The unitary channel currents ($i_j$s) were only discernible at large $V_j$s ($\pm 80$ mV or larger) owing to the low $\gamma_j$ of G46K. All-point histograms were generated from a portion of $i_j$ at the 80 mV $V_j$ and was fitted by two Gaussian functions to obtain the $\gamma_j$ (Fig. 2.4C). The average $\gamma_j$ of G46K channel was $20 \pm 1$ pS (n = 3), which was only about 10% of the Cx50 $\gamma_j$. A representative $i_j$ record at $V_j$ of 80 mV depicted a prolonged open dwell time for each event with occasional transitions to a closed/subconductance state (Fig. 2.4C). Open probability ($P_o$) at this $V_j$ was higher than that of Cx50 channel ($P_o = 0.03$, see Fig. 2.2C). Even at a much higher $V_j$ (120 mV), the G46K channel resided mostly in an open state initially and then the channel was fully closed (Fig. 2.4D). The gating transitions were very slow, usually taking tens of milliseconds or longer (Fig. 2.4D), indicating that the transitions are most likely to be loop gating.
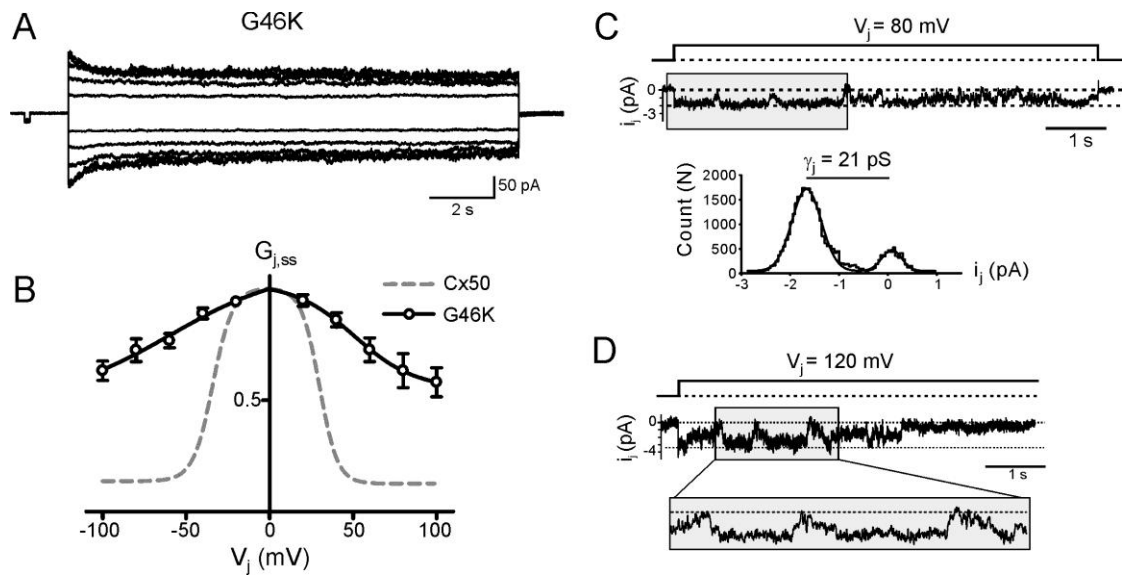
**Fig. 2.4    G46K displays drastically altered $V_j$-gating and single channel properties. A)** A set of macroscopic $I_j$s of G46K GJs in response to $V_j$s of $\pm 20 \sim \pm 100$ mV. **B)** Boltzmann fitting curves of G46K GJs (solid lines) generated from $G_{j,ss}$-$V_j$ plots (n = 6) exhibited lower $V_j$ sensitivities than those of Cx50 GJs (grey dashed lines, same as in Fig. 2.1B). **C)** Single channel current ($i_j$) of a G46K channel at an 80 mV $V_j$ showed a very low $\gamma_j$ (21 pS), which was obtained from the all point histogram analysis of the current trace within the grey box. The closing and opening current levels were indicated by the dotted lines. Despite the frequent transitions to closed state, the dominant state of G46K channel is open state at this $V_j$. **D)** The $i_j$ of a G46K channel at 120 mV $V_j$ showed slow transitions between open and closed states. A portion of the trace is expanded temporally.

### 2.4.5 Heterotypic Cx50/G46K channels displayed asymmetric $V_j$-gating and current rectification

The G46K $V_j$-gating properties are drastically different from those of Cx50 and could be interpreted as a result of the impairment of the fast gating. To test this further, we studied the $V_j$-gating of heterotypic Cx50/G46K channels, in which the docked Cx50 hemichannel is known to have a fast gate (with a positive gating polarity) and a loop gate (with a negative gating polarity) (White *et al.*, 1994; Hopperstad *et al.*, 2000). When applying the Cx50-expressing cell with $+V_j$s (or the G46K cell with $-V_j$s), the recorded $I_j$s showed apparent $V_j$-dependent inactivation (Fig. 2.5A). Conversely, applying $-V_j$s on the Cx50-expressing cells (or $+V_j$s to the G46K-expressing cell) did not cause any perceptible current inactivation (Fig. 2.5A). The $V_j$-gating process during the $+V_j$s on Cx50 side was well fitted by the Boltzmann equation (Fig. 2.5B). A significantly reduced gating sensitivity (*A*) is observed, while other Boltzmann parameters are similar to those of Cx50 channels (Table 2.1).

It is noted that when applying biphasic $V_j$s on the Cx50-expressing cell, the initial amplitudes of the $I_j$s at $+V_j$s was larger than those of corresponding $I_j$s at $-V_j$s (Fig. 2.5A), indicating that the heterotypic Cx50/G46K channels possess a rectifying property. To quantify this, the initial conductance ($G_{j,ini}$) at each $+V_j$ and $-V_j$ were measured, and then the ratio of $G_{j,ini}$ (+) / $G_{j,ini}$ (-) were calculated and plotted to corresponding $V_j$ (Fig. 2.5C). Interestingly, the rectification of heterotypic Cx50/G46K channel is $V_j$-dependent, as the ratio was getting bigger with the increase of $V_j$s (Fig. 2.5C). In contrast, no rectification was observed in the homotypic Cx50

GJs, as the ratios of $G_{j,ini}$ (+) / $G_{j,ini}$ (-) were close to one at different $V_j$s. (Fig. 2.5C).
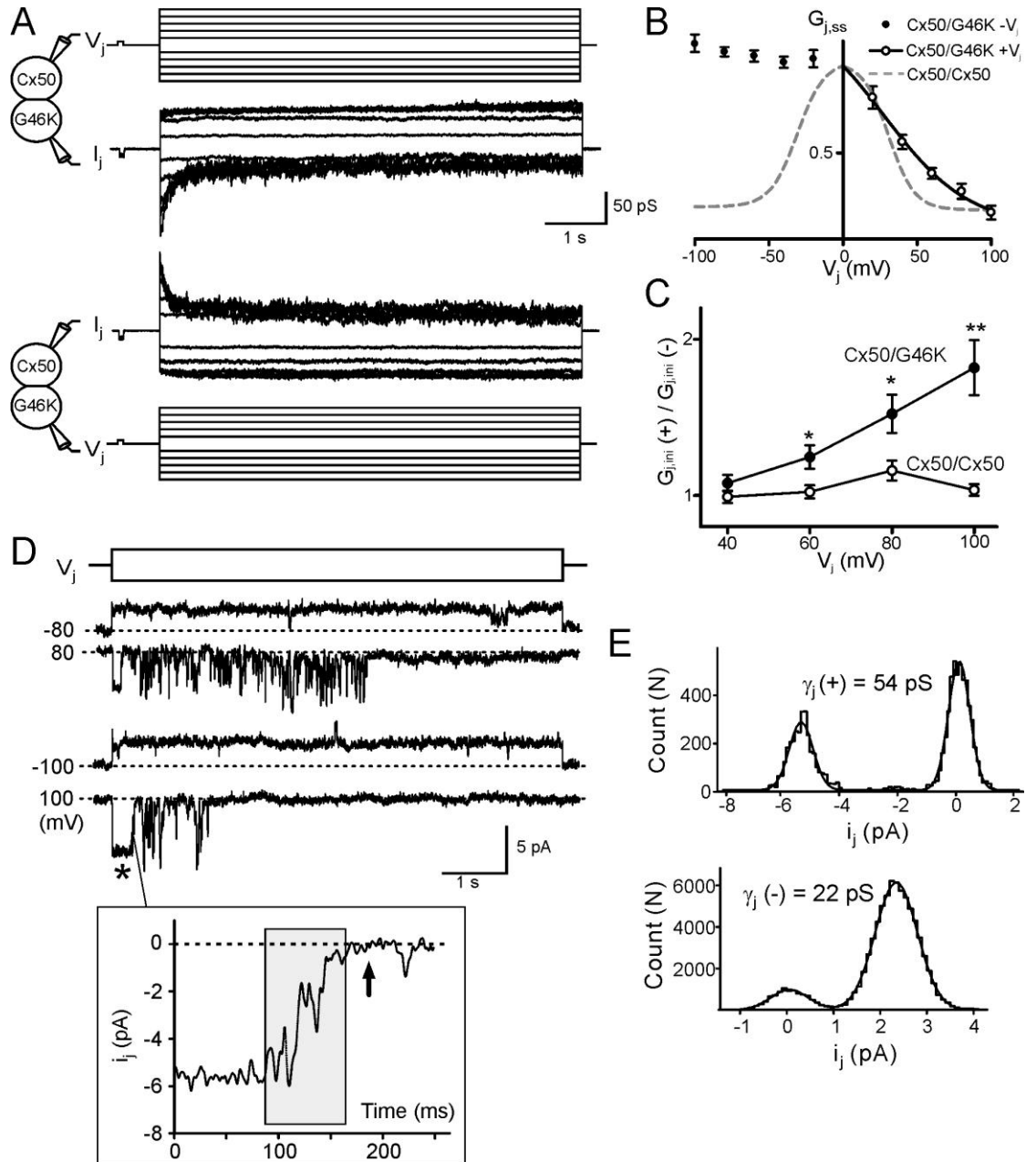
**Fig. 2.5  Heterotypic Cx50/G46K channels show asymmetrical $V_j$-gating and rectification. A)** Two sets of representative $I_j$s of heterotypic Cx50/G46K GJs in response to the $V_j$ protocol ($\pm 20$ mV $\sim \pm 100$ mV) applied to Cx50 expressing cell (top set) or to the G46K expressing cell (bottom set). $I_j$ inactivation was present only when the Cx50 cell with $+V_j$s (or the G46K cell with $-V_j$s). The initial amplitudes of $I_j$s were also different between the corresponding $+V_j$s and $-V_j$s. **B)** The $G_{j,ss}$-$V_j$ plot of heterotypic Cx50/G46K GJs from 6 cell pairs. The smooth line on the $+V_j$s is the Boltzmann fitting curve. At the $-V_j$s, no $V_j$-gating ($I_j$ inactivation) was evident. The Boltzmann fittings of Cx50 channels (grey dashed lines) are shown for comparison. **C)** The initial conductance of $+V_j$s [$G_{j,ini}$ (+)] and $-V_j$s [$G_{j,ini}$ (-)] were calculated and the ratio is plotted to $V_j$. The Cx50/G46K GJs showed a strong $V_j$-dependent rectification. **D)** Heterotypic Cx50/G46K channel showed rectification. The $i_j$s were recorded from the G46K cell in response to $\pm 80$ mV and $\pm 100$ mV $V_j$ pulses (on Cx50-expressing cell). As indicated in the enlarged box below the current, the gating closure reaches fully closed state (pointed by arrow) and the gating transitions typically take tens of ms. **E)** When the Cx50 cell was applied with $+V_j$, the $\gamma_j$ (+) was 54 pS (from an $i_j$ portion at 100 mV indicated by an asterisk). The $\gamma_j$ (-) with $-V_j$ was 22 pS.

**2.4.6   Single heterotypic Cx50/G46K channel showed asymmetric $\gamma_j$ and only slow gating transitions**

Fig. 2.5D illustrates $i_j$s of a heterotypic Cx50/G46K channel in response to $V_j$s. When the holding potential of Cx50-expressing cell was relatively negative to the G46K cell ($-V_j$s), stable $i_j$s were recorded with minimum transitions to any other states. However, when the Cx50-expressing cell was applied with $+V_j$s, the channel was initially open and then became flickering with frequent transitions between the closed/subconductance states and multiple levels of open states, later the channel settled at either a subconductance or the closed state (Fig. 2.5D). A temporal expansion of a portion of $i_j$ revealed that the transition time typically required tens of milliseconds or longer (Fig. 2.5D), indicating that these transitions are likely to be loop gatings. Surprisingly, after carefully going through all the recorded $i_j$ traces at $+V_j$s on the Cx50 side, we found that all discernable gating transitions are very slow and no fast gating transition was spotted. A simple interpretation of these data is that in the heterotypic Cx50/G46K channel, the TM1/E1 border of G46K hemichannel dramatically increased the local resistance for ion permeation, which could consequently cause the $V_j$ redistribution (more on the G46K hemichannel side) and eventually lead to an increase activity of loop gating in the G46K hemichannel.

Parallel to the finding on the $G_{j,ini}$ (+) / $G_{j,ini}$ (-) ratio at the macroscopic level (Fig. 2.5C), the $\gamma_j$ also showed strong rectification on this heterotypic channel at single channel level. The $\gamma_j$ (+), defined as the $\gamma_j$ when Cx50 cell was applied with $+V_j$s, was measured to be 54 pS (Fig. 2.5E). Meanwhile, the $\gamma_j$ (-) (when Cx50 cell was applied

with $-V_j$s) was only 22 pS (Fig. 2.5E). The average data from 4 different heterotypic cell pairs yielded $\gamma_j$ (+) of 50 ± 4 pS and $\gamma_j$ (-) of 24 ± 5 pS (n = 4, p < 0.001). Apparently, these $\gamma_j$ values of Cx50/G46K channels are much lower than the $\gamma_j$ of homotypic Cx50 channel (201 ± 2 pS), but closer to the $\gamma_j$ of homotypic G46K channel (20 ± 1 pS), implying that the G46K hemichannel is likely to be the dominant rate limiting part of this heterotypic channel.

### 2.4.7   G46D failed to alter the ion preference of Cx50 channel

A previous study indicates that Cx50 channels preferentially permeate cations over anions (Srinivas *et al.*, 1999). Introduction of an extra negatively charged residue in the pore lining domain (TM1/E1 border) of each subunit in the channel, such as G46D, would be predicted to have an increase in negative surface charges (6 for each hemichannel and 12 for each GJ channel). This substantial increase in the surface negative charge is predicted to have electrostatic effects on the ions passing through the channel, leading to a possibly higher local cation concentration and a lower anion concentration. To test this hypothesis, we studied the $\gamma_j$s of G46D channel with altered ICFs, which were prepared by replacing the major conducting ions in ICF ($Cs^+$ or $Cl^-$) with much larger sized cations ($TEA^+$) or anions ($Glu^-$), respectively.

As predicted, Cx50 channel showed only a minor reduction (9%) in the $\gamma_j$ when the major electrolyte CsCl was changed to CsGlu (Fig. 2.6A, B; 183 ± 2 pS, n = 4, p < 0.001) and a major reduction (80%) in the $\gamma_j$ when the CsCl was changed to TEACl (41 ± 2 pS, n = 4, p < 0.001), demonstrating indeed that the Cx50 channel has a strong

cation preference. However, G46D channel showed a nearly identical proportional increase (about a quarter) in the $\gamma_j$s using each of the salt solutions comparing to those of Cx50 (Fig. 2.6A and 2.6B), CsCl (256 $\pm$ 5 pS, n = 8), CsGlu (228 $\pm$5, n = 4, p < 0.001) and TEACl (57 $\pm$ 1 pS, n = 4, p < 0.001), while maintaining the same percentage decrease in the $\gamma_j$s (11% in CsGlu and 78% in TEACl), indicating that G46D increased ion permeation without a substantial change in the channel preference on cations.

Same ion preferential experiments were also used to test if G46K GJ channel displays a reduced cation preference. Using CsGlu-based pipette solution, we were able to identify $i_j$s in two cell pairs with $\gamma_j$s of 5 and 8 pS out of more than 40 cell pairs (data not shown). The $\gamma_j$ (with CsGlu) is much lower than that in CsCl (20 $\pm$ 1 pS, n = 4), indicating that G46K channel did indeed show a decrease in the cation preference. However, as it is very difficult to obtain enough data for quantitative comparisons, this observation should be regarded as preliminary. None of the G46K cell pairs showed distinguishable unitary channel currents with TEACl pipette solution, suggesting that either the $\gamma_j$ is too small to be resolved under the experimental conditions or the channel does not have a stable open state.
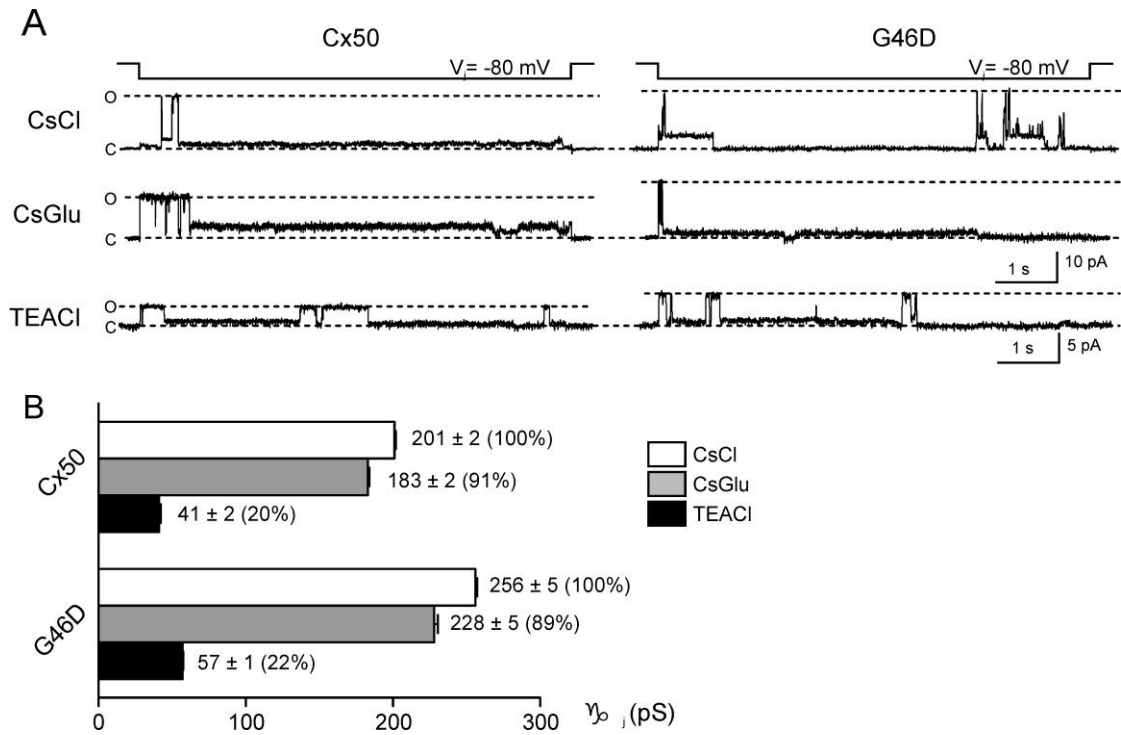
**Fig. 2.6  G46D channel shows a similar ion preference as Cx50. A)** With the substitution of the major salt (either from CsCl to CsGlu or to TEACl) in the pipette solution, single channel recordings of Cx50 and G46D GJ displayed distinctive $\gamma_j$s. The $i_j$s in response to $V_j$ of -80 mV were shown for each type of pipette solution. **B)** The bar graph shows the mean $\gamma_j$s of Cx50 and G46D when using different pipette solutions and their ratios to the control $\gamma_j$s (using CsCl-based pipette solution). All the $\gamma_j$ values were obtained by linear regression of $i_j$-$V_j$ plots.

### 2.4.8  Homology models of Cx50, G46D, G46E and G46K channels

Most connexins have a very high sequence homology with human Cx26, including mouse Cx50 used in the present study. The sequence identity on the crystal structure resolved domains of Cx26 and Cx50 proteins is high (57%), which is sufficient for generating a homology structural model. The initial model of the Cx50 homomeric homotypic channel was generated by using the coordinates of the crystallized Cx26 channel (Maeda *et al.*, 2009). The homology model was then adjusted to eliminate contacts and minimized in energy terms similar to our previous studies (Nakagawa *et al.*, 2011; Gong *et al.*, 2013). The homology models were developed without the knowledge of the experimental results.

The homology model of Cx50 displayed many similar structural properties with that of the crystal structure of Cx26, including the TM1/E1 border domains forming a narrow part of the pore. The homology structures for G46D, G46E and G46K mutants of Cx50 revealed two important structural changes. 1) The channel pore diameter at this position was estimated to be decreased from 20.6 Å for Cx50 to 17.1 Å for G46D, 12.6 Å for G46E and 11.4 Å for G46K on each of the docked hemichannels (Fig. 2.7A). A reduction in the pore diameter could constrict the total number of ions to pass through this pore section and also lead to much closer interactions between the passing ions and the inner surface residues. 2) These mutants displayed a drastic change in the electrostatic potentials at the TM1/E1 border of the channel. As shown in Fig. 2.7B, both G46D and G46E substantially increased the local negativity of electrostatic potential, while G46K created a local narrow ring of positive electrostatic

potential at this domain (Fig. 2.7B). Both the reduced diameter and the ring of positive

electrostatic potential in G46K channel could increase the resistance of the channel to

ions and electrostatically reduce the local cation concentration. The later effect is

predicted to also increase the resistance of this cation-preferring channel. Our

experimental data on the $\gamma_j$ changes of these mutants indicate that the inner surface

charge property of GJ channel is a dominant factor in determining the $\gamma_j$ of Cx50

channel.

Increased local positive electrostatic potential might create a local electrostatic

barrier for permeating cations and substantially decrease the $\gamma_j$ of G46K channel. In

heterotypic Cx50/G46K channel, the asymmetrical electrostatic potentials in the two

docked hemichannels are predicted to contribute to the observed channel rectification.

To explore the possible factors leading to the $V_j$-dependent rectification of heterotypic

Cx50/G46K channel (Fig. 2.5), we inspected the homology structure model of G46K.

The Lys46 (K46) residue contains a long and flexible side chain with a positively

charged amino group at the end. These properties of Lys enable multiple orientations

in response to $V_j$ polarity and intensity. As shown in two possible models with either

$+V_j$ or $-V_j$ on G46K side (Fig. 2.7C), the pore sizes at the Lys46 (K46) position are

different, which could play a role in the observed current rectification of heterotypic

Cx50/G46K channels. At present we could not rule out that other structural changes

might also occur in these mutants, which could provide alternative interpretations to
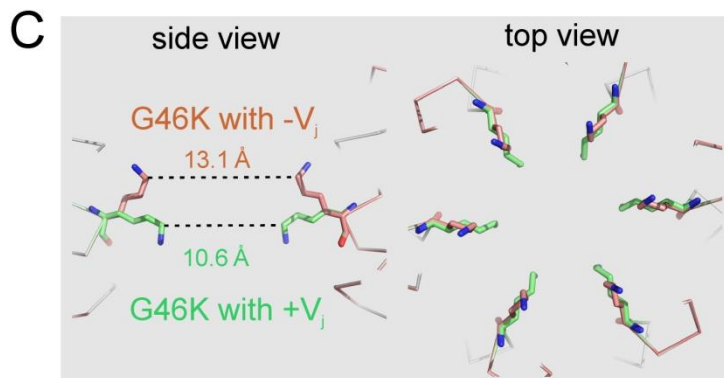
our experimental data.
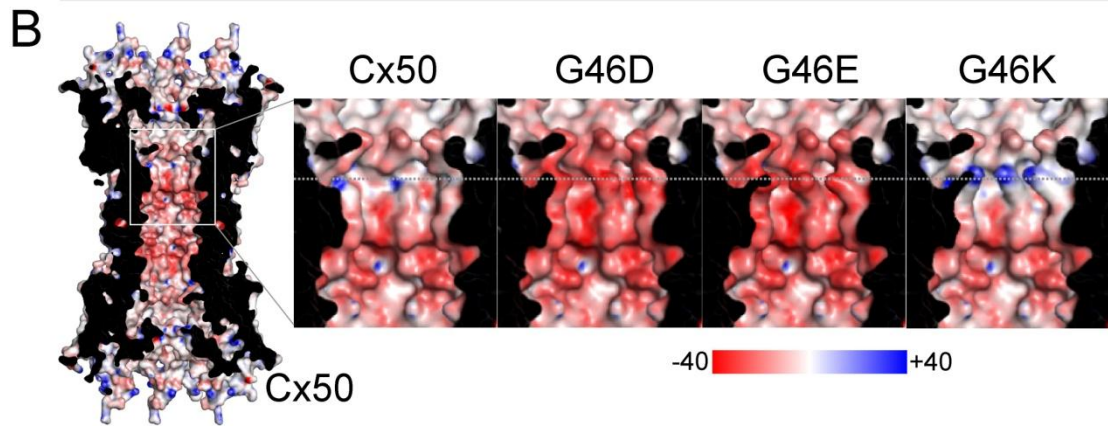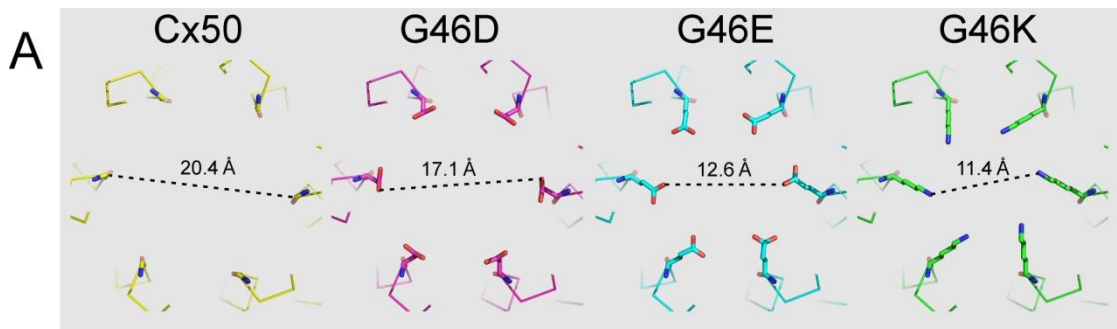
**Fig. 2.7  Homology models of Cx50 and its mutants. A)** Stick view in PyMOL of a portion of the mutant or wild-type Cx50 channels near the 46th residue (top view). The estimated diameters of G46D, G46E and G46K were predicted to decrease as indicated. **B)** A side view of a cut open Cx50 channel is illustrated to show the pore surface electrostatic potentials (calculated with APBS) using dielectric constants of 2 (protein) and 80 (solutions) (Baker *et al.*, 2001). A portion of the Cx50 channel pore surface containing TM1/E1 domains are enlarged as indicated. The electrostatic potentials of the mutant channels at the same position are illustrated. Drastic differences in electrostatic potentials are observed near the mutant residue (dotted horizontal line). The displayed surface electrostatic potentials range from -40 (red) to +40 (blue) kTe-1. **C)** When the G46K-expressing cell was held with different polarity of $V_j$s, two different orientations of Lys46 could be observed and are superimposed in stick view in PyMOL. G46K channel with $-V_j$ (or Cx50 side with $+V_j$ in the heterotypic channel) showed a larger diameter than the G46K channel with $+V_j$, which could play a role in the channel rectification.

## 2.5 Discussion

The present study describes the effects of introducing a negatively/positively charged residue (D, E or K) into the TM1/E1 border domain on the macroscopic and unitary channel properties of the Cx50 GJ channels. G46D/E channel showed little change in the macroscopic $V_j$-gating properties, but significantly increased the $\gamma_j$ and the probability of the channel residing in the fully closed state, while G46K channel displayed drastic changes in both the $V_j$-gating properties and the apparent $\gamma_j$. Heterotypic Cx50/G46K channels showed a strong rectification in both macroscopic and single channel currents. Our homology models indicate that these mutations could change the pore electrostatic properties of the GJ channel, leading to a changed local resistance for the major permeating ions (cations) and a shifted $V_j$ distribution across the whole length of the channel. Altered $V_j$ distribution in the channel in turn could cause apparent changes in fast gating and loop gating properties in these mutants. The charge substitutions in the TM1/E1 border domain were shown to drastically change the $\gamma_j$ from nearly 300 pS (G46E) to an apparent 20 pS (G46K), demonstrating the crucial roles of this domain in determining $\gamma_j$ and $V_j$-gating properties of Cx50 GJ channel.

### 2.5.1 Factors determining the $\gamma_j$ in the mutants

Crucial factors for the efficiency of ion permeation (the $\gamma_j$) through GJ channels are not fully resolved. Here we studied the Cx50 GJ channel with a $\gamma_j$ (200 pS), one of the largest among all characterized GJs (Srinivas *et al.*, 1999; Bai *et al.*, 2006;

Gonzalez *et al.*, 2007; Xin & Bai, 2013). Mutations on the Gly46 to long-side-chained and charged residues (G46D, G46E and G46K) are all likely to decrease the pore size and also alter the electrostatic properties. However, the $\gamma_j$s were actually substantially increased for both G46D (more than a quarter higher) and G46E (almost 50% higher) compared to the Cx50 channel. This result has several implications.

First, the pore size variations of these mutant channels are unlikely to reach any substantial steric hindrance to ion permeation, while the pore surface electrostatic properties could substantially facilitate ion permeation, similar to those described in BK channels (Brelidze *et al.*, 2003; Geng *et al.*, 2011). Considering that the Cx50 channel is a cation-preferring channel, adding 6 x 2 = 12 additional negatively charged residues (D or E) in the permeation pathway would be expected to increase the negativity of the electrostatic potential as shown in Fig. 2.7, perhaps to further facilitate accumulation of local cations and reduction of anions for permeation. However, our data of the $\gamma_j$ reduction with an enlarged cation (TEA$^+$) or anion (Glu$^-$) failed to demonstrate a change in the estimated relative permeability for cations over anions, at least for G46D channel. We also do not know the mechanism for an even higher $\gamma_j$ on G46E channel than that of G46D. Perhaps the longer side chain of Glu46 in the pore is more flexible, which could favor ion permeation.

Second, native Cx50 GJ channel is not fully optimized in its ability to pass ions. A single mutation, G46E, produced an even larger $\gamma_j$, which is almost equal to the $\gamma_j$ of Cx37 channel, the largest among all GJ channels, (Reed *et al.*, 1993; Veenstra *et al.*, 1994; Traub *et al.*, 1998). Detailed comparison of the pore lining residues and their

properties between large $\gamma_j$ channels and low $\gamma_j$ channels may help us to understand more about the ion permeation of these important channels. Understanding the factors controlling ion permeation can offer new avenues for engineering GJs to get enhanced channel function, which can be useful in improving/reestablishing GJ function in many disease-linked connexin mutants (Lee & White, 2009; Beyer *et al.*, 2013; Bai, 2014).

Third, the positively charged residue at the same position, G46K, substantially reduced the apparent $\gamma_j$ to 1/10 of the Cx50. We believe that this again was mainly due to the change of surface electrostatic potentials in the pore. A narrow positively charged ring in the G46K channel is predicted to repel cations and reduce the local cation concentration, which can reduce the $\gamma_j$ of this cation-preferring channel. In addition to this, a substantial reduction in the pore size might also contribute to the reduced $\gamma_j$. Another possible explanation for the low apparent $\gamma_j$ of G46K could be that what we recorded is the subconductance state of the mutant GJ channel rather than the main open state. However, the apparent $\gamma_j$ of G46K was much lower than the conductance of the main subconductance state in Cx50 channel and we never observed a higher $\gamma_j$ level that is comparable to the $\gamma_j$ of Cx50 channel in any of our unitary channel records of homotypic G46K channels and heterotypic Cx50/G46K channels.

Finally, the heterotypic Cx50/G46K channel showed a strong rectification in the $\gamma_j$. This prompted us to look into the potential structural basis. Lys (K) has a positively charged amino group ($-NH_3^+$) at the end of the long flexible side chain. $V_j$ changes

could provide sufficient energy to drive the positively charged amino group to different orientations. Our homology modeling showed that when at different $V_j$s, the side chain of Lys could move to different positions in the pore, causing a reduction/enlargement of the diameter and possibly also the pore surface electrostatic potential. This could be a simple explanation of the observed rectification of the heterotypic Cx50/G46K channel. Obviously, it is too early to rule out the possibility that other structural changes could also play a role in the observed rectification.

### 2.5.2 $V_j$-dependent loop gating was increased in G46D and virtually exclusive in G46K GJs

Previous studies showed that the Cx50 displayed little loop gating in both hemichannel and GJ channel records (Srinivas *et al.*, 1999; Srinivas *et al.*, 2005). Consistent with these early findings, our data on the Cx50 single channel currents rarely display loop gating transition to the fully closed state. When these rare gating events did happen, the channel only showed very brief dwelling at the fully closed state, usually less than a fraction of a second. But G46D (and G46E) channels showed an increased incidence of loop gating and substantially prolonged dwell time in the fully closed state, which significantly increased the probability of the channel in the closed state. The increased stability of closed state was accompanied by a reduced probability of the open state and subconductance state, especially during the high $V_j$s. When the $V_j$s were at $\pm100$ mV, a portion of G46D (and G46E) channels were dwelled in the fully closed state at the end of $V_j$ pulse, making the data of macroscopic

$G_{j,ss}$-$V_j$ plot consistently below the fitting curves.

Different from what observed in G46D/E, G46K channels drastically changed macroscopic $V_j$-gating properties. The $V_j$-gating was virtually eliminated, this was well-described by the changes in Boltzmann parameters: $G_{min}$s were more than 4 fold higher and *A* values were reduced to ~1/3 of those of Cx50 channels. Studies on the single G46K channel revealed a substantially reduced $\gamma_j$, which is likely due to the mutation-created electrical barrier for permeating ions at the TM1/E1 border of the pore. Such electrical barrier is expected to increase the $V_j$ drop across this region of the GJ pore and cause a $V_j$-redistribution at the other pore sections, which could increase the sensitivity of the loop gating sensor and decrease the sensitivity of the fast gating sensor. Such a model can also be used to explain our data on heterotypic Cx50/G46K channels, where K46 position on the mutant hemichannel would have the highest resistance of the entire GJ channel, which would not only dictate the $\gamma_j$, but also receive the majority of the $V_j$. In addition, this $V_j$ redistribution would reduce the $V_j$ drop on the fast gate sensors of both Cx50 and G46K hemichannels, causing an apparent loss of fast gating in this heterotypic GJ channel. This model is a simple plausible interpretation of our experimental data.

### 2.5.3   TM1/E1 border domain is a hotspot for human disease-linked mutations

Mutations in several connexin genes are linked to inherited human diseases, including cataract (Cx50 and Cx46) (Beyer *et al.*, 2013) and non-syndromic and syndromic deafness (Cx26) (Lee & White, 2009). Many of these mutants are clustered

around the TM1/E1 border (Lee & White, 2009; Beyer *et al.*, 2013), indicating that the residues at this domain are important for normal GJ function in these connexins. Several mutations happened directly on the G46 (or equivalent) residue. G46R and G46V of the Cx50 were found to be linked to cataract (Minogue *et al.*, 2009; Sun *et al.*, 2011). *In vitro* expression study on G46V revealed that this mutant caused cell death possibly due to increased hemichannel activities (Minogue *et al.*, 2009). In Cx26, G45E mutant (equivalent to G46 in Cx50) was found to be linked to keratitis-ichthyosis-deafness syndrome (KIDS) (Janecke *et al.*, 2005; Griffith *et al.*, 2006). In an in-vitro expression system, G45E was found to be expressed at a similar level as wild-type Cx26 and formed a similar level of GJ coupling (Gerido *et al.*, 2007), while the $V_j$-gating properties of its GJ channels were changed (a decrease in the $V_0$) (Gerido *et al.*, 2007; Sanchez *et al.*, 2010) and the single hemichannel conductance was increased by ~25% (Sanchez *et al.*, 2010). The increase in the single hemichannel conductance of G45E is consistent with our finding. However, we did not observe any obvious change of the $V_j$-gating properties in either Cx50-G46E or G46D, indicating that the $V_j$-gating sensor and/or the $V_j$-distribution of the Cx50 channel are likely to be different from those of Cx26. Whether the biophysical changes in Cx26-G45E GJ channel contribute to the disease burden are not fully resolved, but could be an additive factor to the proposed key disease-causing mechanism, the increased hemichannel function (Stong *et al.*, 2006; Gerido *et al.*, 2007; Sanchez *et al.*, 2010; Mese *et al.*, 2011).

## 2.5.4 Structure-function study of Cx50-G46 equivalent residues in other connexins

Early studies identified that the pore-lining TM1/E1 border domain plays important roles in normal physiological functions, such as gating and $Ca^{2+}$-sensing, and mutations at this domain are associated with serious diseases (Verselis *et al.*, 1994; Oh *et al.*, 1999; Trexler *et al.*, 2000; Gomez-Hernandez *et al.*, 2003; Janecke *et al.*, 2005; Griffith *et al.*, 2006; Minogue *et al.*, 2009). A detailed systematical mapping of all the residues within this domain was carried out on Cx46 hemichannel and found that the Gly46 is one of the crucial residues in determining the single hemichannel conductance of Cx46. Similar to our findings on the Cx50 GJ channels, introducing a positively charged residue (such as Lys, Arg, or Cys which is then modified by positively charged methanethiosulfonate [MTS] reagents) at the Gly46 position substantially reduced the single hemichannel conductance (Kronengold *et al.*, 2003). However, the introduction of a negatively charged residue in Cx46 hemichannel, which was realized by modifying G46C mutation with negatively charged methanethiosulfonate (MTS-ES⁻), did not increase the single hemichannel conductance (Kronengold *et al.*, 2003), possibly due to the reason that the MTS-ES⁻ on Cys is much larger than the side chain of Glu⁻ or Asp⁻ (making the channel smaller) or Cx46 could be a much less cation-preferring channel compared to Cx50. Consistent with our findings on the altered $\gamma_j$s of Cx50 mutants, Cx26 G45C showed qualitatively similar hemichannel conductance changes after reacting to positively or negatively charged MTS reagents (Sanchez *et al.*, 2010). Hemichannel studies on Cx26-G45E or

equivalent mutants in Cx30, Cx32 and Cx43 have shown the importance of this position in stabilizing the fully closed state of their hemichannels with the assistance of extracellular $Ca^{2+}$ or other divalent cations (Sanchez *et al.*, 2010; Zhang & Hao, 2013). These studies and our results argue a significant role for the TM1/E1 border domain in the biophysical properties of GJ channels.

## 2.6    Acknowledgments

## 2.7 References

Bai D. (2014). Atrial fibrillation-linked GJA5/connexin40 mutants impaired gap junctions via different mechanisms. FEBS Lett 588, 1238.

Bai D, del Corsso C, Srinivas M & Spray DC. (2006). Block of specific gap junction channel subtypes by 2-aminoethoxydiphenyl borate (2-APB). J Pharmacol Exp Ther 319, 1452-1458.

Baker NA, Sept D, Joseph S, Holst MJ & McCammon JA. (2001). Electrostatics of nanosystems: application to microtubules and the ribosome. Proc Natl Acad Sci U S A 98, 10037-10041.

Beyer EC, Ebihara L & Berthoud VM. (2013). Connexin mutants and cataracts. Front Pharmacol 4, 43.

Brelidze TI, Niu X & Magleby KL. (2003). A ring of eight conserved negatively charged amino acids doubles the conductance of BK channels and prevents inward rectification. Proc Natl Acad Sci U S A 100, 9017-9022.

Bukauskas FF, Elfgang C, Willecke K & Weingart R. (1995). Biophysical properties of gap junction channels formed by mouse connexin40 in induced pairs of transfected human HeLa cells. Biophys J 68, 2289-2298.

DeLano WL. (2006). The PyMOL Molecular Graphics System. v.0.99.

Dong L, Liu X, Li H, Vertel BM & Ebihara L. (2006). Role of the N-terminus in permeability of chicken connexin45.6 gap junctional channels. J Physiol 576, 787-799.

Ek-Vitorin JF & Burt JM. (2005). Quantification of gap junction selectivity. Am J Physiol Cell Physiol 289, C1535-1546.

Geng Y, Niu X & Magleby KL. (2011). Low resistance, large dimension entrance to the inner cavity of BK channels determined by changing side-chain volume. J Gen Physiol 137, 533-548.

Gerido DA, DeRosa AM, Richard G & White TW. (2007). Aberrant hemichannel properties of Cx26 mutations causing skin disease and deafness. Am J Physiol Cell Physiol 293, C337-345.

Gomez-Hernandez JM, de Miguel M, Larrosa B, Gonzalez D & Barrio LC. (2003). Molecular basis of calcium regulation in connexin-32 hemichannels. Proc Natl Acad Sci U S A 100, 16030-16035.

Gong XQ, Nakagawa S, Tsukihara T & Bai D. (2013). A mechanism of gap junction docking revealed by functional rescue of a human-disease-linked connexin mutant. J Cell Sci 126, 3113-3120.

Gong XQ & Nicholson BJ. (2001). Size selectivity between gap junction channels composed of different connexins. Cell Commun Adhes 8, 187-192.

Gonzalez D, Gomez-Hernandez JM & Barrio LC. (2007). Molecular basis of voltage dependence of connexin channels: an integrative appraisal. Prog Biophys Mol Biol 94, 66-106.

Goodenough DA & Paul DL. (2009). Gap junctions. Cold Spring Harb Perspect Biol 1, a002576.

Griffith AJ, Yang Y, Pryor SP, Park HJ, Jabs EW, Nadol JB, Jr., Russell LJ, Wasserman DI, Richard G, Adams JC & Merchant SN. (2006). Cochleosaccular dysplasia associated with a connexin 26 mutation in keratitis-ichthyosis-deafness syndrome. <u>Laryngoscope</u> 116, 1404-1408.

Hille B. (2001). Ion channels of excitable membrane. Sinauer Associates, Inc., Massachusetts.

Hopperstad MG, Srinivas M & Spray DC. (2000). Properties of gap junction channels formed by Cx46 alone and in combination with Cx50. <u>Biophys J</u> 79, 1954-1966.

Janecke AR, Hennies HC, Gunther B, Gansl G, Smolle J, Messmer EM, Utermann G & Rittinger O. (2005). GJB2 mutations in keratitis-ichthyosis-deafness syndrome including its fatal form. <u>Am J Med Genet</u> A 133A, 128-131.

Kronengold J, Trexler EB, Bukauskas FF, Bargiello TA & Verselis VK. (2003). Single-channel SCAM identifies pore-lining residues in the first extracellular loop and first transmembrane domains of Cx46 hemichannels. <u>J Gen Physiol</u> 122, 389-405.

Lee JR & White TW. (2009). Connexin-26 mutations in deafness and skin disease. <u>Expert Rev Mol Med</u> 11, e35.

Maeda S, Nakagawa S, Suga M, Yamashita E, Oshima A, Fujiyoshi Y & Tsukihara T. (2009). Structure of the connexin 26 gap junction channel at 3.5 A resolution. <u>Nature</u> 458, 597-602.

Mese G, Sellitto C, Li L, Wang HZ, Valiunas V, Richard G, Brink PR & White TW. (2011). The Cx26-G45E mutation displays increased hemichannel activity in a mouse model of the lethal form of keratitis-ichthyosis-deafness syndrome. <u>Mol Biol Cell</u> 22, 4776-4786.

Minogue PJ, Tong JJ, Arora A, Russell-Eggitt I, Hunt DM, Moore AT, Ebihara L, Beyer EC & Berthoud VM. (2009). A mutant connexin50 with enhanced hemichannel function leads to cell death. <u>Invest Ophthalmol Vis Sci</u> 50, 5837-5845.

Nakagawa S, Gong XQ, Maeda S, Dong Y, Misumi Y, Tsukihara T & Bai D. (2011). Asparagine 175 of connexin32 is a critical residue for docking and forming functional heterotypic gap junction channels with connexin26. <u>J Biol Chem</u> 286, 19672-19681.

Oh S, Rubin JB, Bennett MV, Verselis VK & Bargiello TA. (1999). Molecular determinants of electrical rectification of single channel conductance in gap junctions formed by connexins 26 and 32. <u>J Gen Physiol</u> 114, 339-364.

Reed KE, Westphale EM, Larson DM, Wang HZ, Veenstra RD & Beyer EC. (1993). Molecular cloning and functional expression of human connexin37, an endothelial cell gap junction protein. <u>J Clin Invest</u> 91, 997-1004.

Saez JC, Berthoud VM, Branes MC, Martinez AD & Beyer EC. (2003). Plasma membrane channels formed by connexins: their regulation and functions. <u>Physiol Rev</u> 83, 1359-1400.

Sanchez HA, Mese G, Srinivas M, White TW & Verselis VK. (2010). Differentially altered Ca2+ regulation and Ca2+ permeability in Cx26 hemichannels formed by the A40V and G45E mutations that cause keratitis ichthyosis deafness syndrome.

J Gen Physiol 136, 47-62.

Sanchez HA, Villone K, Srinivas M & Verselis VK. (2013). The D50N mutation and syndromic deafness: altered Cx26 hemichannel properties caused by effects on the pore and intersubunit interactions. J Gen Physiol 142, 3-22.

Simon AM & Goodenough DA. (1998). Diverse functions of vertebrate gap junctions. Trends Cell Biol 8, 477-483.

Sohl G & Willecke K. (2004). Gap junctions and the connexin protein family. Cardiovasc Res 62, 228-232.

Srinivas M, Costa M, Gao Y, Fort A, Fishman GI & Spray DC. (1999). Voltage dependence of macroscopic and unitary currents of gap junction channels formed by mouse connexin50 expressed in rat neuroblastoma cells. J Physiol 517, 673-689.

Srinivas M, Kronengold J, Bukauskas FF, Bargiello TA & Verselis VK. (2005). Correlative studies of gating in Cx46 and Cx50 hemichannels and gap junction channels. Biophys J 88, 1725-1739.

Stong BC, Chang Q, Ahmad S & Lin X. (2006). A novel mechanism for connexin 26 mutation linked deafness: cell death caused by leaky gap junction hemichannels. Laryngoscope 116, 2205-2210.

Sun W, Xiao X, Li S, Guo X & Zhang Q. (2011). Mutational screening of six genes in Chinese patients with congenital cataract and microcornea. Mol Vis 17, 1508-1513.

Tang Q, Dowd TL, Verselis VK & Bargiello TA. (2009). Conformational changes in a pore-forming region underlie voltage-dependent "loop gating" of an unapposed connexin hemichannel. J Gen Physiol 133, 555-570.

Traub O, Hertlein B, Kasper M, Eckert R, Krisciukaitis A, Hulser D & Willecke K. (1998). Characterization of the gap junction protein connexin37 in murine endothelium, respiratory epithelium, and after transfection in human HeLa cells. Eur J Cell Biol 77, 313-322.

Trexler EB, Bukauskas FF, Kronengold J, Bargiello TA & Verselis VK. (2000). The first extracellular loop domain is a major determinant of charge selectivity in connexin46 channels. Biophys J 79, 3036-3051.

Veenstra RD, Wang HZ, Beblo DA, Chilton MG, Harris AL, Beyer EC & Brink PR. (1995). Selectivity of connexin-specific gap junctions does not correlate with channel conductance. Circ Res 77, 1156-1165.

Veenstra RD, Wang HZ, Beyer EC, Ramanan SV & Brink PR. (1994). Connexin37 forms high conductance gap junction channels with subconductance state activity and selective dye and ionic permeabilities. Biophys J 66, 1915-1928.

Verselis VK, Ginter CS & Bargiello TA. (1994). Opposite voltage gating polarities of two closely related connexins. Nature 368, 348-351.

Verselis VK, Trelles MP, Rubinos C, Bargiello TA & Srinivas M. (2009). Loop Gating of Connexin Hemichannels Involves Movement of Pore-lining Residues in the First Extracellular Loop Domain. J Biol Chem 284, 4484-4493.

Weber PA, Chang HC, Spaeth KE, Nitsche JM & Nicholson BJ. (2004). The permeability of gap junction channels to probes of different size is dependent on

connexin composition and permeant-pore affinities. <u>Biophys J</u> 87, 958-973.

White TW, Bruzzone R, Wolfram S, Paul DL & Goodenough DA. (1994). Selective interactions among the multiple connexin proteins expressed in the vertebrate lens: the second extracellular domain is a determinant of compatibility between connexins. <u>J Cell Biol</u> 125, 879-892.

Wilders R & Jongsma HJ. (1992). Limitations of the dual voltage clamp method in assaying conductance and kinetics of gap junction channels. <u>Biophys J</u> 63, 942-953.

Xin L & Bai D. (2013). Functional roles of the amino terminal domain in determining biophysical properties of Cx50 gap junction channels. <u>Front Physiol</u> 4, 373.

Xin L, Gong XQ & Bai D. (2010). The role of amino terminus of mouse Cx50 in determining transjunctional voltage-dependent gating and unitary conductance. <u>Biophys J</u> 99, 2077-2086.

Zhang Y & Hao H. (2013). Conserved glycine at position 45 of major cochlear connexins constitutes a vital component of the Ca(2)(+) sensor for gating of gap junction hemichannels. <u>Biochem Biophys Res Commun</u> 436, 424-429.

# Chapter 3: Discussion

## 3.1 Overall study

This study investigated the effects of introducing a negatively (D or E) or positively (K) charged residue into the G46 position of Cx50, in order to explore the role of the TM1/E1 border domain in determining $\gamma_j$, $V_j$-dependent gating and cation/anion preference of Cx50 GJ channels. Specifically, the G46D/E mutants showed significantly increased $\gamma_j$, while the G46K mutant showed startlingly reduced $\gamma_j$. Moreover, the noteworthy changes of $V_j$-gating in the single channel records of G46D/E GJ channel are shortened dwell time in the main open state and prolonged dwell time in the fully closed state. In the G46K GJ channels, it is likely that the fast gating is abolished and the loop gating activity becomes more prominent. By comparing the homology models of Cx50 GJ channel and its mutants, it is predicted that these changes are closely related to the surface electrostatic potential of the TM1/E1 border in these channels.

The TM1/E1 border is a newly described domain which may be a loop gating sensor and/or gate in both hemichannels and GJ channels (Kronengold, Trexler et al. 2003; Tang, Dowd et al. 2009; Verselis, Trelles et al. 2009; Lopez, Liu et al. 2014). In the Cx26 GJ channel, negatively charged residues in this domain are lining the pore surface, which construct a special section with a highly negative electrostatic potential (Maeda, Nakagawa et al. 2009). Sequence alignment revealed that negatively charged residues in this domain are highly conserved in other connexins. However, the role of

this domain in determining GJ properties has not been fully addressed. Our study will help illustrate the contribution of the TM1/E1 border to the Cx50 GJ properties.

## 3.2   Preliminary experiments on E1 domain of Cx50

A chimeric construct Cx50Cx36E1, which was generated by replacing the entire E1 domain of Cx50 with that of Cx36, was studied in our preliminary experiments (data not shown). The purpose of studying this chimera is to explore the role of E1 domain in determining the properties of Cx50 and Cx36 GJ channels. Cx50 and Cx36 GJ channels showed remarkable discrepancies in their $V_j$ gating properties and $\gamma_j$s. Cx50 GJ channels are highly sensitive to $V_j$ and their $\gamma_j$ is around 200 pS (Srinivas, Costa et al. 1999), whereas Cx36 channels show little $V_j$-dependence and their $\gamma_j$ is only ~6-15 pS (Srinivas, Rozental et al. 1999; Moreno, Berthoud et al. 2005). Therefore, they are two perfect candidates to study the structure-function relationship of GJ channels. Previous studies in our lab, using domain swapping and single-point substitutions between Cx50 and Cx36, found that the NT domain of Cx50 (especially its two residues D3 and N9) is critical in determining $\gamma_j$ and $V_j$ gating properties of Cx50 GJ channel (Xin, Gong et al. 2010; Xin, Nakagawa et al. 2012).

In addition to NT, E1 domain is also suggested as a component of the interior channel wall. Surprisingly, Cx50Cx36E1 GJ channels showed almost the same $V_j$-gating properties as Cx50, and their mean $\gamma_j$ was only reduced by around 20% compared to that of Cx50 (data not shown). Since the replacement of the whole E1 domain has the potential to cause global changes to the structure of Cx50 GJ channel, it is hard to interpret the results without a specific crystal structure for the chimera.

## 3.3 Surface charges at the TM1/E1 border impact single channel conductance

In this thesis, GJ channels of G46D and G46E exhibited considerably increased $\gamma_j$ by nearly 25% and 50%, while G46K GJ channels showed a 90% drop in $\gamma_j$. The homology models of Cx50 GJ channel and its mutants depicted the differences in both the pore size of the G46 position and the surface electrostatic field of the TM1/E1 border, which provide possible structural interpretations for our data.

Firstly, it is noticed that $\gamma_j$s of Cx50, G46D and G46E GJ channels are not proportional to the predicted pore diameters at the TM1/E1 border in their homology models. The local pore diameters of these three channels are predicted to be gradually reduced, yet their $\gamma_j$s are increased progressively. A message we draw from this observation is that a larger pore size at the TM1/E1 border may not guarantee a higher $\gamma_j$ at least in Cx50 GJ channels. Moreover, it provides a new clue to explain previous observations that some GJ channels (e.g. Cx50, Cx37 and Cx40) with big $\gamma_j$s exhibited low permeability to fluorescent dyes (Veenstra, Wang et al. 1994; Veenstra, Wang et al. 1995; Veenstra 1996). For instance, the $\gamma_j$ of Cx37 GJ channels is around 300 pS, the largest among all tested connexin subunits, yet the ability of this channel to pass fluorescence dyes is much lower than that of other GJ channels (e.g. Cx43 and Cx45) whose $\gamma_j$s are around 100 pS and 30 pS, respectively (Veenstra, Wang et al. 1995). A simple explanation is that a relatively smaller pore size at the TM1/E1 border may facilitate the interaction between passing ions and fixed pore surface charges, which would subsequently facilitate ion flow and yield high $\gamma_j$. But on the other hand, the

channel becomes less permeable to various fluorescent dyes whose molecular weights, usually above 300 Da, are much bigger in size than those of ions.

Secondly, according to the homology models, the negative electrostatic field at the TM1/E1 border was strengthened in G46D/E channels compared to that of Cx50, but was much weakened in G46K channels. Matching these properties to their $\gamma_j$s, it is likely to suggest that a pure and strong negative electrostatic field at the TM1/E1 border would optimize ion permeability through the long GJ channel, which is probably also associated with the cation-preferring property of Cx50 channels. Previous studies in different GJ channels observed similar effects on $\gamma_j$ when altering the surface residues at the TM1/E1 border (Kronengold, Trexler et al. 2003; Tong and Ebihara 2006). A representative example is the Cx26-G45E hemichannel ( a mutant at the G45 position of Cx26), which showed 25% increase in its hemichannel $\gamma_j$ compared to wild-type Cx26 hemichannel, whereas another mutant Cx26-D50N exhibited 50% lower $\gamma_j$ (Sanchez, Mese et al. 2010; Sanchez, Villone et al. 2013). Considering that Cx26 channels favor cations to pass through just like Cx50 (Suchyna, Nitsche et al. 1999) and both G45 and D50 are pore-lining residues at the TM1/E1 border, the opposite effects between G45E and D50N are in agreement with the conjecture that adding a negative surface charge into the TM1/E1 border (Cx26-G45E) increased the $\gamma_j$ of Cx26 GJ channels, while removing one (Cx26-D50N) from the inner pore surface decreased the $\gamma_j$ as a consequence.

## 3.4 Do surface charges at the TM1/E1 border play a role in determining cation/anion preference?

Of all documented GJ channels to date, almost all prefer the passage of cations rather than anions, except Cx32 GJ channels, which have a slight anion preference (Suchyna, Nitsche et al. 1999; Gonzalez, Gomez-Hernandez et al. 2007). The key role of E1 domain in determining cation/anion preference of a connexin channel has been identified in a few connexins, such as Cx46, whose cation-preferring property was reversed by replacing its E1 domain with that of Cx32 (Trexler, Bukauskas et al. 2000). Moreover, studies on Cx32 channels revealed the contribution of both E1 and NT domains to its anion-preferring property, especially their pore-lining charged residues (Oh, Verselis et al. 2008). Therefore, unlike potassium and sodium channels, GJ channels do not seem to have a particular selective filter and its ion preference is largely determined by surface charges in the current pathway. In our study (chapter 2, Fig. 2.6), despite that G46D GJ channel is predicted to have a much stronger negative electrostatic field at the TM1/E1 border than Cx50, its $\gamma_j$ tested with TEACl or CsGlu-based ICF showed a similar reduction ratio as those of Cx50. It is likely to suggest that a stronger negative electrostatic potential at the TM1/E1 border of G46D channels facilitate the cationic and anionic flows simultaneously rather than the cationic flow alone. It is difficult to provide a satisfactory explanation based on our current knowledge of GJ channels. A possible reason is that the TM1/E1 border of Cx50 channels already contains abundant negative surface charges as indicated in the homology model, thus the addition of an extra negative charge (G46D) may only exert

limited effects.

## 3.5 A possible explanation for instantaneous current rectification in heterotypic Cx50/G46K channels.

Previous studies have observed pronounced rectification mostly in heterotypic GJ channels, such as Cx32/Cx26, Cx31/Cx26, Cx31/Cx30 and Cx43/Cx45 (Verselis, Ginter et al. 1994; Bukauskas, Angele et al. 2002; Abrams, Freidin et al. 2006). The rectification of Cx32/Cx26 heterotypic channel was ascribed to the asymmetric ion permselectivities and conductances of its two opposed hemichannels (Suchyna, Nitsche et al. 1999). Structural studies on Cx32 and Cx26 identified the NT and E1 domains, especially the asymmetric distribution of charged residues in these two domains, as the major determinants of channel rectification (Rubin, Verselis et al. 1992; Oh, Rubin et al. 1999). Since these two domains construct the intracellular entrance and the extracellular exit of a hemichannel respectively, it is reasonable that their abilities to accumulate and deplete ions are critical for the channel conductance.

In our study, very strong instantaneous current rectification was observed in both macroscopic and single channel records of heterotypic Cx50/G46K channels (Chapter 2, Fig. 2.5). With the application of a positive $V_j$ ($+V_j$) on the Cx50 side, the channel $\gamma_j$ is about twice as much as the value when applying a negative $V_j$ ($-V_j$) on the Cx50 side, indicative of an unequal ability of the channel to conduct ions in opposite directions. As discussed in Chapter 2, the homology model of G46K demonstrated two different orientations of Lys (K) side chain driven by the bipolar $V_j$s, which

would result in different local pore diameters and distorted electrostatic potentials within the pore. Both these two factors would eventually lead to different $\gamma_j$s in opposite $V_j$ polarities. This mechanism could be one of multiple causes of the channel rectification.

Another feature of the Cx50/G46K channel is that the rectification is $V_j$-dependent. At $\pm 20$ mV and $\pm 40$ mV pulses, the initial conductance at positive $V_j$ [$G_{j,ini}$ (+) ] was almost identical to the initial conductance at negative $V_j$ [$G_{j,ini}$(-)], but their difference increases with increasing $V_j$ (Chapter 2, Fig. 2.5A&C), indicating that the conducting ability of the hetrotypic channel was enhanced when applying higher $+V_j$ on the Cx50 side, and weakened when applying higher $-V_j$ on the Cx50 side. This phenomenon was only described once in an early study on Cx26/Cx32 heterotypic channel without pointing out the underlying mechanism (Bukauskas, Elfgang et al. 1995). In the homology model of G46K (Chapter 2, Fig. 2.7C), although merely two orientations of Lys (K) side chain at positive and negative $V_j$s were posited, we should bear in mind that not only the Lys (K) side chain would adopt multiple orientations at different $V_j$s, but also the structure of the whole channel may be dynamic rather than static when permeating ions and other substances.

## 3.6 Surface charges at the TM1/E1 border influence loop gating behavior

Very limited evidence has been accumulated regarding the determinants for loop gating behavior. Kronengold and colleagues reported that replacing the whole

NT-TM1-E1 domain of Cx50 with that of Cx46 evidently enhanced the occurrence of loop gating in Cx50 hemichannels, a feature resembling Cx46 hemichannels (Kronengold, Srinivas et al. 2012). In our studies, the sole replacement of G46 with a positively charged Lys (K) in Cx50 made loop gating surpass fast gating to become a dominant gating in response to $V_j$ pulses. One possibility for this observation is that the fast gate of G46K channel is always closed, which would reduce the channel conductance to a subconductance level and eradicate the fast gating activities during the $V_j$ application. However, up-to-date knowledge convinces that the fast gating of most studied GJ channels (except Cx40 and Cx43) is governed by NT domain (Verselis, Ginter et al. 1994; Purnick, Oh et al. 2000; Oh, Rivkin et al. 2004; Oh, Verselis et al. 2008) and little evidence shows the structural interaction between NT and TM1/E1 border. Thereby, it seems unlikely that a mutant at the TM1/E1 border would damage the open state of NT and put it into a closed state. Further tests on the heterotypic coupling of Cx50 and G46K hemichannels provide extra support to rule out this possibility. Fig. 3.1 illustrates the possible positions of two fast gates and two loop gates in a Cx50/G46K GJ channel under different $V_j$ conditions in accordance with the single channel records of the heterotypic Cx50/G46K channel in Chapter 2 (Fig. 2.5D). In our opinion, only the loop gate of G46K hemichannel responds to the negative $V_j$ on the G46K side, while the fast gate in neither Cx50 nor G46K hemichannel can be triggered by biphasic $V_j$s. It implies that the G46K hemichannel is capable of abolishing the fast gating not only on its own side but also in the opposed Cx50 hemichannel. As the $V_j$ sensors for fast and loop gatings are proposed to lie in

the pore for the purpose of sensing $V_j$ directly, their activities should be governed by the voltage drop across the sensors. In this case, it is reasonable to assume that the disappearance of fast gating in both homotypic G46K/G46K and heterotypic Cx50/G46K channels is more likely to be the consequence of $V_j$ redistribution rather than a direct damage to the fast gate structure in each hemichannel. In a G46K GJ channel, the coexistence of negative and positive surface charges at the TM1/E1 border increases the local electrostatic resistance to both cations and anions, which would substantially raise the voltage drop at this position and make the loop gating sensor more readily to respond. In short, introducing a positively charged residue to G46 makes the TM1/E1 border a much more sensitive voltage sensor for the loop gating and is unlikely to change the conformation of fast gate sensor/gate in the NT domain.
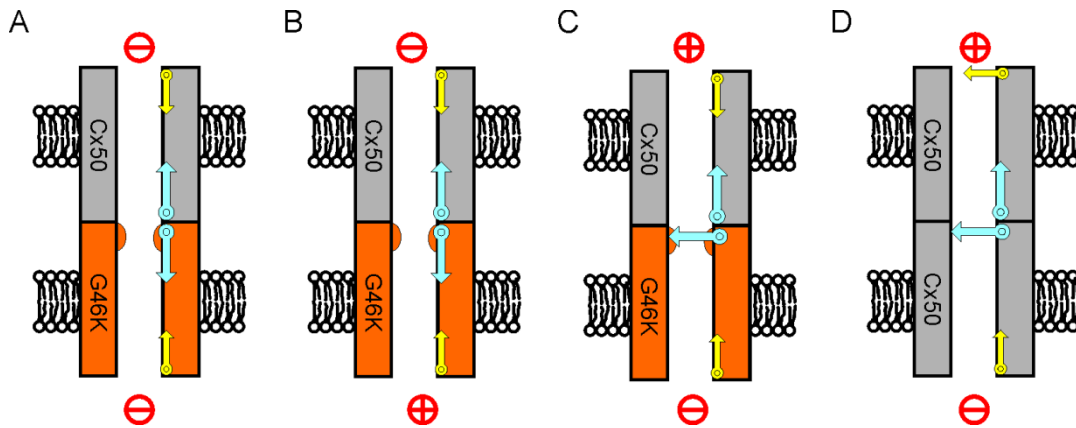
**Figure 3.1   A possible mechanism for the abolished fast gating in Cx50/G46K heterotypic GJ channel. A**) A cartoon diagram showing the profile of a heterotypic GJ channel docked by Cx50 (grey) and G46K (orange) hemichannels. Note that the TM1/E1 border is narrower in the G46K hemichannel than in the Cx50 hemichannel, indicating a physical and electrical barrier to ion flow. The channel keeps opening without $V_j$ administration. B) Imposing positive $V_j$ on the G46K side fails to close any gates because most $V_j$ drop is imposed at the TM1/E1 border of the G46K hemichannel, but the loop gate at this location only responds to the intracellular negative potential. C) When applying sufficient negative $V_j$ on the G46K side, loop gate of the G46K hemichannel is closed but fast gate of the Cx50 hemichannel cannot be shut down due to the low $V_j$ drop on it. D) When the same $V_j$ condition as in C) is applied on a homotypic Cx50 GJ channel, both fast gate of the top Cx50 hemichannel and loop gate of the bottom Cx50 hemichannel have a chance to be closed, but the fast gate is much more sensitive than the loop gate.

## 3.7 The role of G45/46 position in hemichannel function

For Cx26, as well as Cx30, Cx32 and Cx43, its mutant G45E (equivalent to G46E in Cx50) demonstrated increased hemichannel current compared to wild type at depolarizing voltage and this leaky current through hemichannels was restored by increasing extracellular $Ca^{2+}$ concentration (Gerido, DeRosa et al. 2007; Mese, Sellitto et al. 2011; Zhang and Hao 2013). Studies suggested that a stable closure of the loop gating in an undocked hemichannel includes two essential steps. Firstly, an inside negative potential ($V_m$ in this case) would drive the conformation reorganization at the TM1/E1 border and result in the approaching of 6 parahelix structures to the pore center to close the hemichannel. Secondly, the closed state of the hemichannel is stabilized by high-concentration extracellular $Ca^{2+}$, which is possibly achieved by the interactions between $Ca^{2+}$ and the proximate metal binding residues in the parahelices (Gomez-Hernandez, de Miguel et al. 2003; Verselis and Srinivas 2008; Tang, Dowd et al. 2009; Zhang and Hao 2013). Furthermore, Lopez and colleagues reported that other than acting as a stabilizer, extracellular $Ca^{2+}$ also aimed to break a salt bridge between residues D50 and K61 in the Cx26 hemichannel and collapse the channel at the extracellular end (Lopez, Gonzalez et al. 2013). Although there is no direct evidence showing that the loop gating behavior in a hemichannel is different from that after docking to the other hemichannel, here we raise a concern over the conformations of the closed state in a hemichannel and a GJ channel. In our study, GJ channels of G46D and G46E exhibit increased stability at fully closed state compared to wild-type Cx50 as long-lived dwelling at the fully closed sate was frequently recorded (Chapter

2, Fig 2.2). So what decides the stability of the fully closed state in a GJ channel? Given that in a GJ channel, the TM1/E1 border is buried deeply in the middle and the docking interface of two hemichannels is likely to be tightly sealed (Foote, Zhou et al. 1998; Maeda and Tsukihara 2011), it seems unlikely that the TM1/E1 border would have access to abundant extracellular $Ca^{2+}$. Therefore, we doubt whether the fully closed state in a GJ channel would adopt the same mechanism as that of a hemichannel, using extracellular $Ca^{2+}$ to assist the break-down of the open state of loop gate and the stabilization of fully closed state. Certainly, more research is needed to clarify this question.

## 3.8   Limitations and future plans

This study yields several novel views in terms of the role of TM1/E1 border in determining $\gamma_j$ and $V_j$-gating properties of Cx50 GJ channels. However, the limitations on current knowledge of GJ channels and techniques we used make it hard to fully interpret our results. Firstly, the shortage of high-resolution crystal structures for the Cx50 GJ channel in any states (open, subconductance or closed) makes it difficult to correlate our observations to corresponding conformational changes. Up to date, the only available high resolution crystal structure is a 3.5 Å human Cx26 GJ channel at its open state. As GJ channels demonstrated a lot of common features, such as their sensitivities to $V_j$ and intracellular pH, their two $V_j$-gating components (fast gating and loop gating), the same pore-lining domains (NT-TM1-E1 domain) proved in various connexins and the ability of NT residues to determine $V_j$ gating properties, it

seems more likely that their overall structures would be similar to each other. We carefully compared the sequence identity and homology of the crystal structure resolved domains between Cx26 and Cx50 before generating a homology model for Cx50 GJ channel. Even so, without an experimentally determined high resolution structure for Cx50 GJ channel, it is not clear if a residue alteration at the G46 position would result in an overall structural change of the whole channel since the newly added amino acid D/E or K at this position may establish extra non-covalent interactions with neighboring residues. Therefore, a high resolution structure of the Cx50 GJ channel would increase the understanding of our functional data.

Another concern is the method we used in the study. Site-directed mutagenesis and domain exchange between connexins are two routine approaches to explore the structure-function relationship of GJ channels and are productive in revealing putative pore-lining residues/domains, as well as a few inter-subunit and intra-subunit interactions. Most of these results are highly consistent with the crystal structure of Cx26 GJ channel. Nonetheless, the prerequisite for these methods to generate useful information is that modified connexins are still capable of forming functional GJ channels. A counter example is the Cx50-D51M mutant we tested in a preliminary study. D51 is also suggested as a pore lining residue at the TM1/E1 border of Cx50 GJ channel (Verselis, Trelles et al. 2009), but its mutant D51M doesn't seem to form functional GJ channels (data not shown). Several possible reasons arose: 1) low level expression of D51M mutant in transfected N2A cells; 2) inefficient oligomerization in ER or Golgi; 3) failed trafficking to the plasma membrane; 4) unsuccessful docking to

81

an opposed hemichannel; 5) successful docking but failed opening. Further immunostaining tests with Cx50 antibodies would help eliminate some of these possibilities, but little useful information regarding its structure-function correlations can be attained from this Cx50-D51M mutant via patch-clamp approach.

This study suggests that surface charges at the TM1/E1 border of Cx50 GJ channels contribute to its $V_j$-gating characteristics and $\gamma_j$. Due to the highly conserved sequence identity of this domain among different connexins, our future plan is to validate this theory on other connexins. We are also interested in exploring the abnormal functions of two cataract-linked mutants Cx50-G46V and G46R in two aspects: $V_j$-gating and permeability of their GJ channels (Minogue, Tong et al. 2009; Sun, Xiao et al. 2011). Valine (V) is a non-charged hydrophobic amino acid with an alkyl side chain and arginine (R) possesses an extremely bulky side chain. If one of them is placed in the channel pore, the mutated channel may exhibit significantly altered $\gamma_j$ and $V_j$ gating. Meanwhile, G46R/V theoretically could form heteromeric and heterotypic GJ channels with wild-type Cx50 and/or Cx46 due to the physiologically co-localization of these connexins in lens, thus a mutation in Cx50 could have dominant negative effects on wild-type Cx50 and/or transdominant negative effects on co-expressed Cx46 to change the intracellular communications in lens, which might eventually lead to cataract.

## 3.9    Summary

By mutating G46 to charged residues, we revealed essential roles of charges on the pore lining residues at the TM1/E1 border in determining $\gamma_j$ and $V_j$-gating properties of Cx50 GJ channels, probably by modifying the efficiency of ion flow through the pore and properly allocating the $V_j$ along different parts of the whole channel. Clearly, the high density negative surface charges at the TM1/E1 border of Cx50 GJ channel could reduce the local resistance, most likely by facilitating cation flow, as cations are the major components of passing ions via this channel.

Interestingly, in physiological conditions, most second messengers (e.g. cAMP, cGMP and IP3) and metabolites (e.g. ATP, ADP and glutamate) are anionic and their molecular weights are as big as hundreds of Daltons. The cation-preferring property of almost all GJ channels may finely regulate passage of these anionic molecules, which are responsible for many physiological functions in the cells. Despite the overall similarity in cation/anion preference, each type of GJ channel has distinct permeability to intracellular substances, which is largely determined by the structure and the electrostatic properties of the pore surface. The TM1/E1 border appears to be an important site to determine the channel permeability to ions and other charged molecules and also to fully close the channel via the loop gating mechanism in Cx50 and possibly other GJ channels.

## 3.10 References

Abrams, C. K., M. M. Freidin, et al. (2006). "Properties of human connexin 31, which is implicated in hereditary dermatological disease and deafness." <u>Proc Natl Acad Sci U S A</u> **103**(13): 5213-5218.

Bukauskas, F. F., A. B. Angele, et al. (2002). "Coupling asymmetry of heterotypic connexin 45/ connexin 43-EGFP gap junctions: properties of fast and slow gating mechanisms." <u>Proc Natl Acad Sci U S A</u> **99**(10): 7113-7118.

Bukauskas, F. F., C. Elfgang, et al. (1995). "Heterotypic gap junction channels (connexin26-connexin32) violate the paradigm of unitary conductance." <u>Pflugers Arch</u> **429**(6): 870-872.

Foote, C. I., L. Zhou, et al. (1998). "The pattern of disulfide linkages in the extracellular loop regions of connexin 32 suggests a model for the docking interface of gap junctions." <u>J Cell Biol</u> **140**(5): 1187-1197.

Gerido, D. A., A. M. DeRosa, et al. (2007). "Aberrant hemichannel properties of Cx26 mutations causing skin disease and deafness." <u>Am J Physiol Cell Physiol</u> **293**(1): C337-345.

Gomez-Hernandez, J. M., M. de Miguel, et al. (2003). "Molecular basis of calcium regulation in connexin-32 hemichannels." <u>Proc Natl Acad Sci U S A</u> **100**(26): 16030-16035.

Gonzalez, D., J. M. Gomez-Hernandez, et al. (2007). "Molecular basis of voltage dependence of connexin channels: an integrative appraisal." <u>Prog Biophys Mol Biol</u> **94**(1-2): 66-106.

Kronengold, J., M. Srinivas, et al. (2012). "The N-terminal half of the connexin protein contains the core elements of the pore and voltage gates." <u>J Membr Biol</u> **245**(8): 453-463.

Kronengold, J., E. B. Trexler, et al. (2003). "Single-channel SCAM identifies pore-lining residues in the first extracellular loop and first transmembrane domains of Cx46 hemichannels." <u>J Gen Physiol</u> **122**(4): 389-405.

Lopez, W., J. Gonzalez, et al. (2013). "Insights on the mechanisms of Ca(2+) regulation of connexin26 hemichannels revealed by human pathogenic mutations (D50N/Y)." <u>J Gen Physiol</u> **142**(1): 23-35.

Lopez, W., Y. Liu, et al. (2014). "Divalent regulation and intersubunit interactions of human Connexin26 (Cx26) hemichannels." <u>Channels (Austin)</u> **8**(1): 1-4.

Maeda, S., S. Nakagawa, et al. (2009). "Structure of the connexin 26 gap junction channel at 3.5A resolution." <u>Nature</u> **458**(7238): 597-602.

Maeda, S. and T. Tsukihara (2011). "Structure of the gap junction channel and its implications for its biological functions." <u>Cell Mol Life Sci</u> **68**(7): 1115-1129.

Mese, G., C. Sellitto, et al. (2011). "The Cx26-G45E mutation displays increased hemichannel activity in a mouse model of the lethal form of keratitis-ichthyosis-deafness syndrome." <u>Mol Biol Cell</u> **22**(24): 4776-4786.

Minogue, P. J., J. J. Tong, et al. (2009). "A mutant connexin50 with enhanced hemichannel function leads to cell death." <u>Invest Ophthalmol Vis Sci</u> **50**(12):

5837-5845.

Moreno, A. P., V. M. Berthoud, et al. (2005). "Biophysical evidence that connexin-36 forms functional gap junction channels between pancreatic mouse beta-cells." Am J Physiol Endocrinol Metab **288**(5): E948-956.

Oh, S., S. Rivkin, et al. (2004). "Determinants of gating polarity of a connexin 32 hemichannel." Biophys J **87**(2): 912-928.

Oh, S., J. B. Rubin, et al. (1999). "Molecular determinants of electrical rectification of single channel conductance in gap junctions formed by connexins 26 and 32." J Gen Physiol **114**(3): 339-364.

Oh, S., V. K. Verselis, et al. (2008). "Charges dispersed over the permeation pathway determine the charge selectivity and conductance of a Cx32 chimeric hemichannel." J Physiol **586**(10): 2445-2461.

Purnick, P. E., S. Oh, et al. (2000). "Reversal of the gating polarity of gap junctions by negative charge substitutions in the N-terminus of connexin 32." Biophys J **79**(5): 2403-2415.

Rubin, J. B., V. K. Verselis, et al. (1992). "Molecular analysis of voltage dependence of heterotypic gap junctions formed by connexins 26 and 32." Biophys J **62**(1): 183-193; discussion 193-185.

Sanchez, H. A., G. Mese, et al. (2010). "Differentially altered Ca2+ regulation and Ca2+ permeability in Cx26 hemichannels formed by the A40V and G45E mutations that cause keratitis ichthyosis deafness syndrome." J Gen Physiol **136**(1): 47-62.

Sanchez, H. A., K. Villone, et al. (2013). "The D50N mutation and syndromic deafness: altered Cx26 hemichannel properties caused by effects on the pore and intersubunit interactions." J Gen Physiol **142**(1): 3-22.

Srinivas, M., M. Costa, et al. (1999). "Voltage dependence of macroscopic and unitary currents of gap junction channels formed by mouse connexin50 expressed in rat neuroblastoma cells." J Physiol **517 ( Pt 3)**: 673-689.

Srinivas, M., R. Rozental, et al. (1999). "Functional properties of channels formed by the neuronal gap junction protein connexin36." J Neurosci **19**(22): 9848-9855.

Suchyna, T. M., J. M. Nitsche, et al. (1999). "Different ionic selectivities for connexins 26 and 32 produce rectifying gap junction channels." Biophys J **77**(6): 2968-2987.

Sun, W., X. Xiao, et al. (2011). "Mutational screening of six genes in Chinese patients with congenital cataract and microcornea." Mol Vis **17**: 1508-1513.

Tang, Q., T. L. Dowd, et al. (2009). "Conformational changes in a pore-forming region underlie voltage-dependent "loop gating" of an unapposed connexin hemichannel." J Gen Physiol **133**(6): 555-570.

Tong, J. J. and L. Ebihara (2006). "Structural determinants for the differences in voltage gating of chicken Cx56 and Cx45.6 gap-junctional hemichannels." Biophys J **91**(6): 2142-2154.

Trexler, E. B., F. F. Bukauskas, et al. (2000). "The first extracellular loop domain is a major determinant of charge selectivity in connexin46 channels." Biophys J **79**(6): 3036-3051.

Veenstra, R. D. (1996). "Size and selectivity of gap junction channels formed from different connexins." J Bioenerg Biomembr **28**(4): 327-337.

Veenstra, R. D., H. Z. Wang, et al. (1995). "Selectivity of connexin-specific gap junctions does not correlate with channel conductance." Circ Res **77**(6): 1156-1165.

Veenstra, R. D., H. Z. Wang, et al. (1994). "Connexin37 forms high conductance gap junction channels with subconductance state activity and selective dye and ionic permeabilities." Biophys J **66**(6): 1915-1928.

Verselis, V. K., C. S. Ginter, et al. (1994). "Opposite voltage gating polarities of two closely related connexins." Nature **368**(6469): 348-351.

Verselis, V. K. and M. Srinivas (2008). "Divalent cations regulate connexin hemichannels by modulating intrinsic voltage-dependent gating." J Gen Physiol **132**(3): 315-327.

Verselis, V. K., M. P. Trelles, et al. (2009). "Loop gating of connexin hemichannels involves movement of pore-lining residues in the first extracellular loop domain." J Biol Chem **284**(7): 4484-4493.

Xin, L., X. Q. Gong, et al. (2010). "The role of amino terminus of mouse Cx50 in determining transjunctional voltage-dependent gating and unitary conductance." Biophys J **99**(7): 2077-2086.

Xin, L., S. Nakagawa, et al. (2012). "Aspartic acid residue D3 critically determines Cx50 gap junction channel transjunctional voltage-dependent gating and unitary conductance." Biophys J **102**(5): 1022-1031.

Zhang, Y. and H. Hao (2013). "Conserved glycine at position 45 of major cochlear connexins constitutes a vital component of the Ca(2)(+) sensor for gating of gap junction hemichannels." Biochem Biophys Res Commun **436**(3): 424-429.

# XIAOLING TONG

**Master Candidate, Physiology and Pharmacology**, University of Western Ontario, Canada (2012 - present)

**Master, Medical Immunology**, Wuhan University, Wuhan, China (2006 - 2008)
Chinese National Scholarship (2006 - 2008)

**Bachelor, Clinical Medicine**, Wuhan University, Wuhan, China (2001 - 2006)
Second Class Scholarship for Outstanding Student, China (2001- 2006)

## EMPLOYMENT EXPERIENCE

**UNIVERSITY OF WESTERN ONTARIO,** London, ON
2012 - Present **Research Assistant**

**UNIVERSITY OF WESTERN ONTARIO,** London, ON
2013 - 2014
**Graduate Teaching Assistant for Cellular Physiology Course**

**USCN LIFE SCIENCE, INC.,** Wuhan, China
2008 - 2012
**Manager of Technique Support Department** (2009 - 2012)
**Technician of Technique Support Department** (2008 - 2009)

## CONFERENCE ABSTRACTS & PRESENTATIONS

1. **Tong, X**., Aoyama, H., Tsukihara, T. and Bai, D. (2014) Charge at the 46th residue of Cx50 is critical for the gap junction channel unitary conductance and transjunctional voltage-dependent gating. 2014 International Biophysics Congress, Brisbane, Australia (abstract submitted)

2. **Tong, X**. and Bai, D. (2014) Positively and negatively charged residues at position 46 in Cx50 have different effects on unitary conductance and transjunctional voltage dependent gating. London Health Research Day, London, Canada (poster presentation)

3. **Tong, X**. and Bai, D. (2014) The residues in the first extracellular domain play an important role in transjunctional-voltage dependent gating and unitary conductance of Cx50 gap junction channels. Biophysical Society 58th Annual Meeting, San Francisco, California (poster presentation)

## PUBLICATIONS

1. **Tong, X.,** Aoyama, H., Tsukihara, T. and Bai, D. (2014) Charge at the 46th residue of Cx50 is critical for the gap junctional unitary conductance and transjunctional voltage-dependent gating. Submitted.

2. Sun, Y., Hills, M.D., Ye, W.G., **Tong, X.** and Bai, D. (2014) Atrial Fibrillation-Linked Germline GJA5/Connexin 40 Mutants Showed an Increased Hemichannel Function. PLOS ONE 9(4): e95125.

3. Sun, Y., **Tong, X.**, Chen, H., Huang, T., Shao, Q., Huang, W., Laird, D.W. and Bai, D. (2014) An endoplasmic reticulum-retained atrial fibrillation-linked Connexin40 mutant impairs atrial gap junction channel function. Dis Model Mech.

4. Zhang, L., Yu, B., Hu, M., Wang, Z., Liu, D., **Tong, X.**, Leng, J., Zhou, B., Hu, Y., Wu, R. Ding, Q. and Zhang, Q. (2011) Role of Rho-ROCK signaling in MOLT4 cells metastatis induced by CCL25. Leuk Res 35(1): 103-109.

5. Zhou, B., Leng, J., Hu, M., Zhang, L., Wang, Z., Liu, D., **Tong, X.**, Yu, B., Hu, Y., Deng, C., Liu, Y. and Zhang, Q. (2010) Ezrin is a key molecule in the metastasis of MOLT4 cells induced by CCL25/CCR9. Leuk Res 34(6): 769-776.

6. **Tong, X.,** Zhang, L., Hu, M., Leng, J., Yu, B., Zhou, B., Hu, Y. and Zhang, Q. (2009) The mechanism of chemokine receptor 9 internalization triggered by interleukin 2 and interleukin 4. Cell Mol Immunol 6(3): 818-189.

## INTERNSHIP

**GENDA BIOTECH.,** Guangzhou**,** China
2008.6 - 2008.11

**Assistant in R&D Department**


**ZHONGNAN HOSPITAL**, Wuhan, China
2005.7 - 2006.7

**Intern Doctor**